APPENDIX E - FIGURES

List of Figures 1.1 - 3.76 on pages xi-xvi

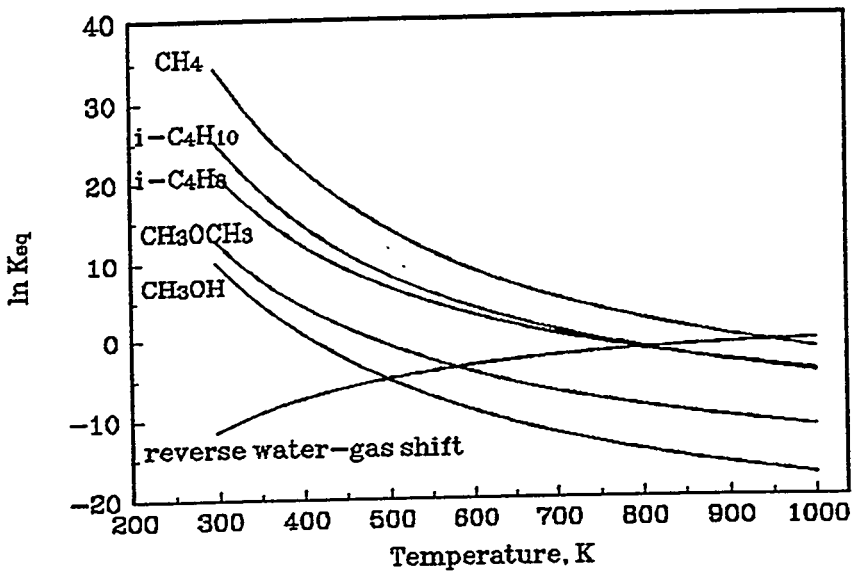

Figure 1.1. Temperature dependence of equilibrium constants. Hydrogenation of CO is exothermic.

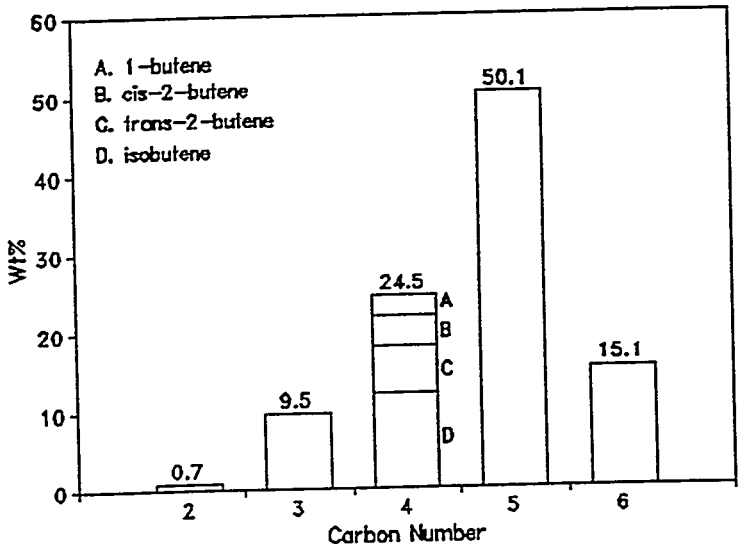

Figure 1.2. Equilibrium distributions of alkenes from hydrogenation of CO at 700 K, 70 atm, and 1/1 CO/H_2 ratio.

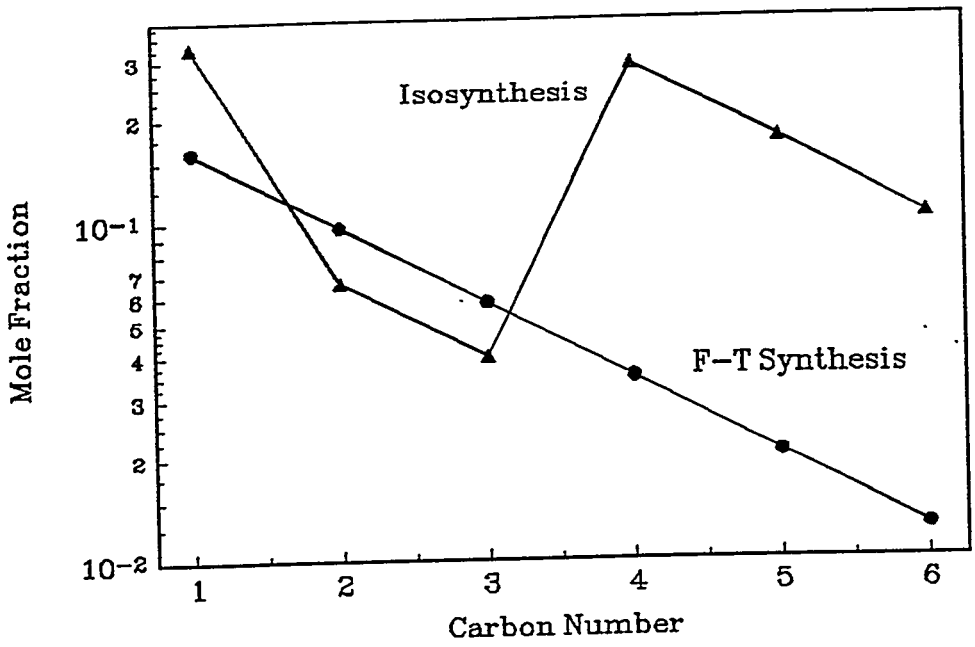

Figure 1.3. The Schulz-Flory-Anderson plots for the distributions of hydrocarbons. ▲: Isosynthesis (*4*); ●: F-T synthesis (*28*).

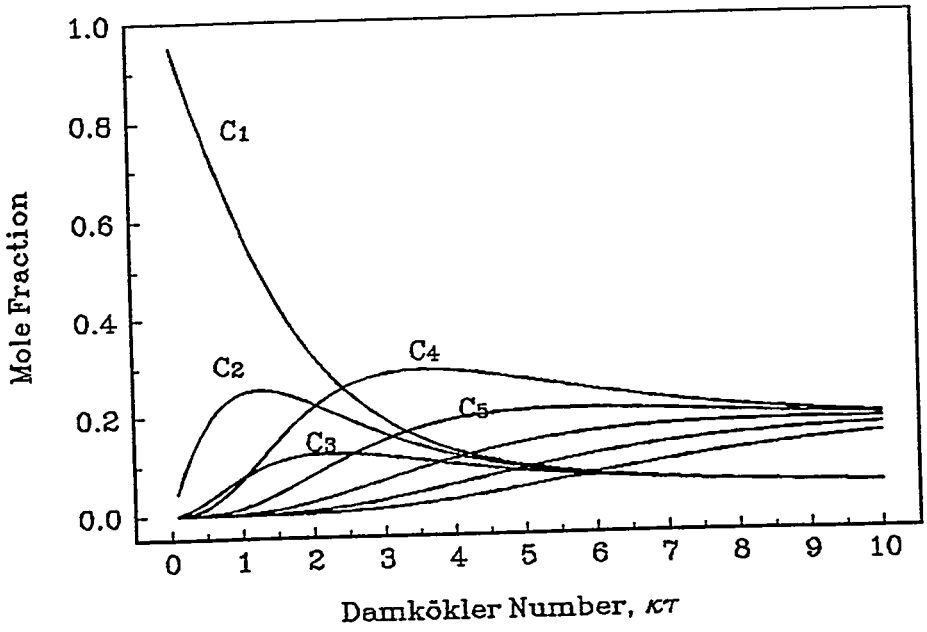

Figure 1.4. Distribution of C_1 to C_8 hydrocarbons as a function of space time.

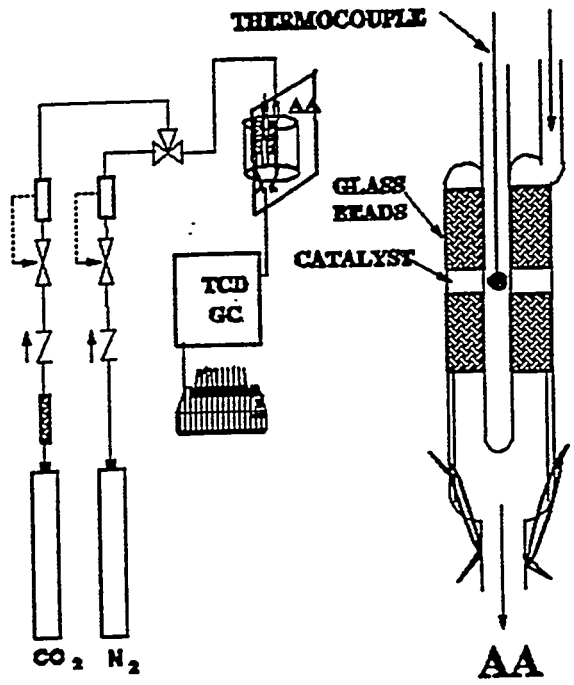

Figure 2.1. Schematic diagram of TPD apparatus.

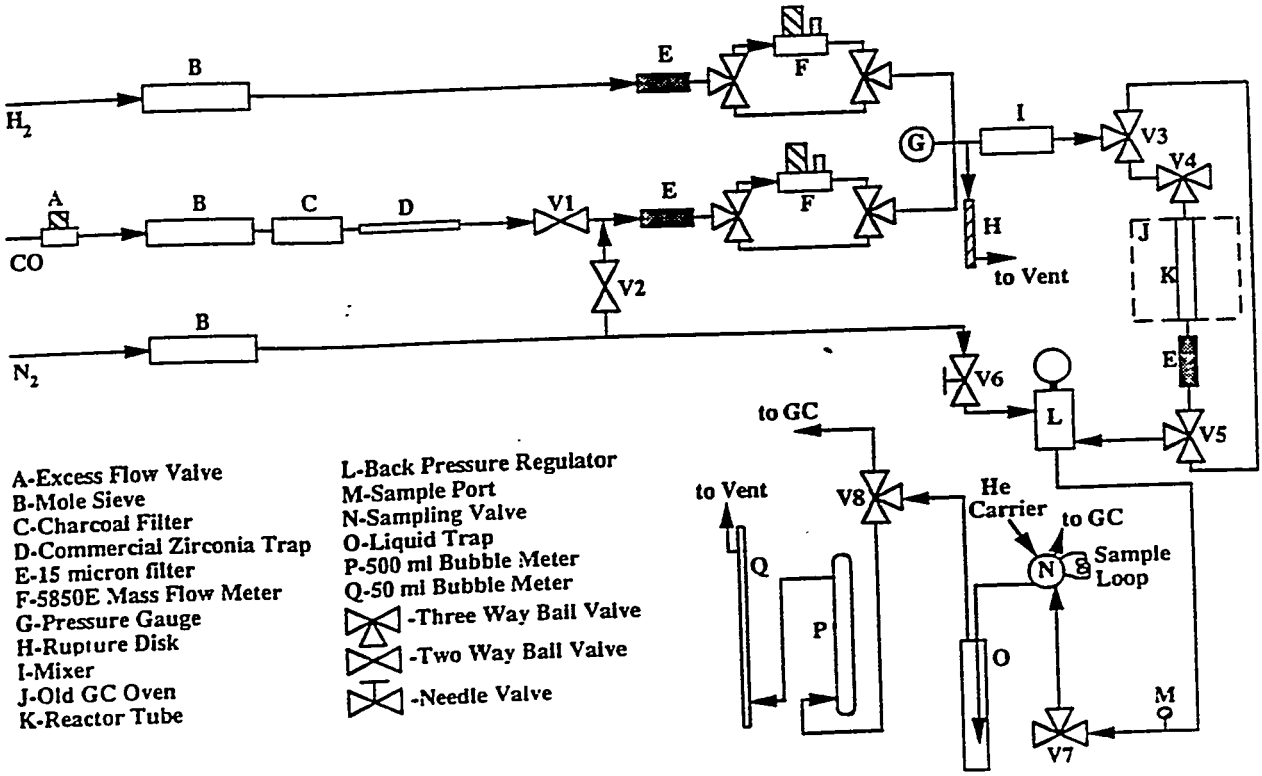

Figure 2.2. Schematic diagram of fixed bed reactor system 1.

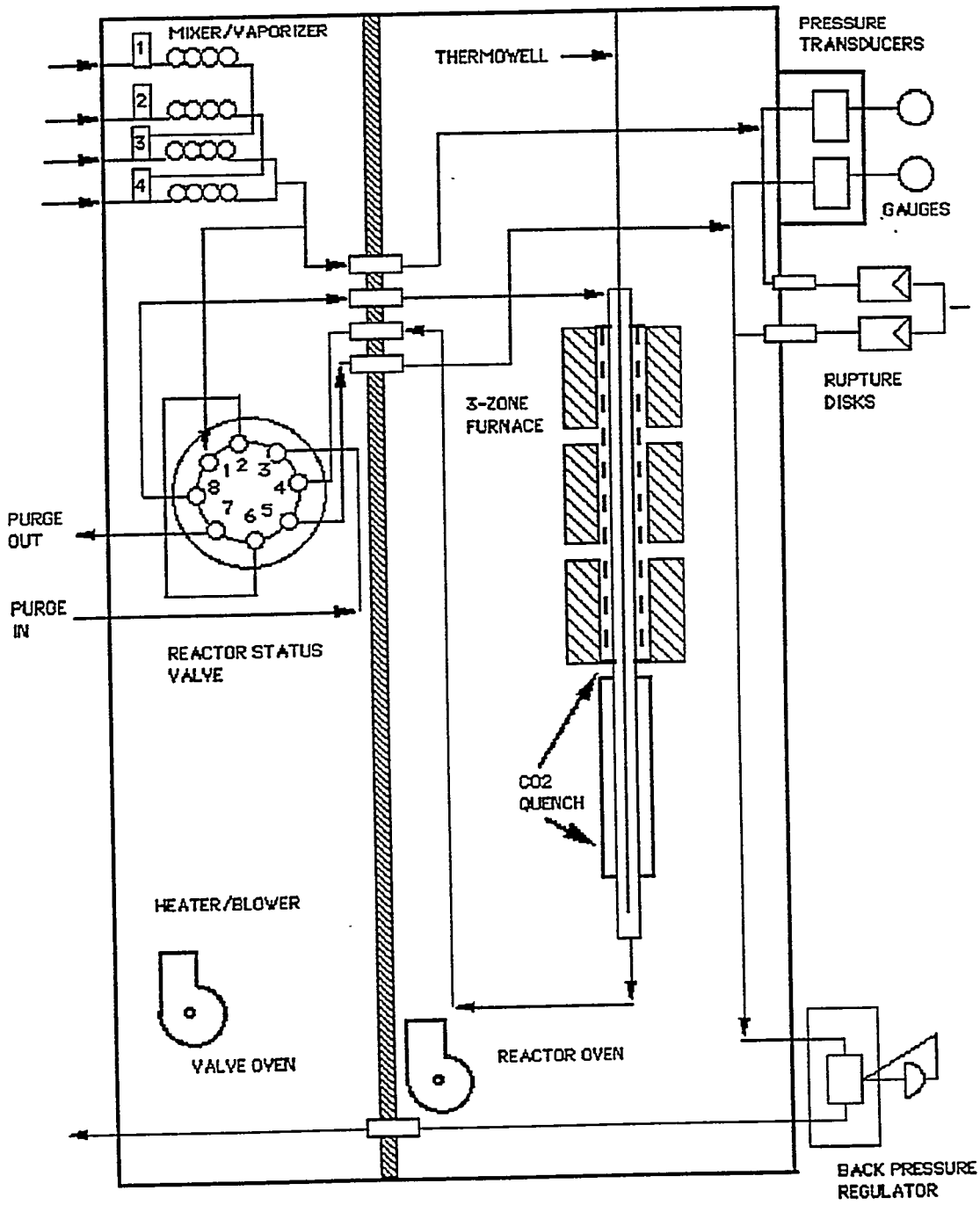

Figure 2.3. CDS 900 Micro-scale bench-top reaction system (Fixed bed reactor 2).

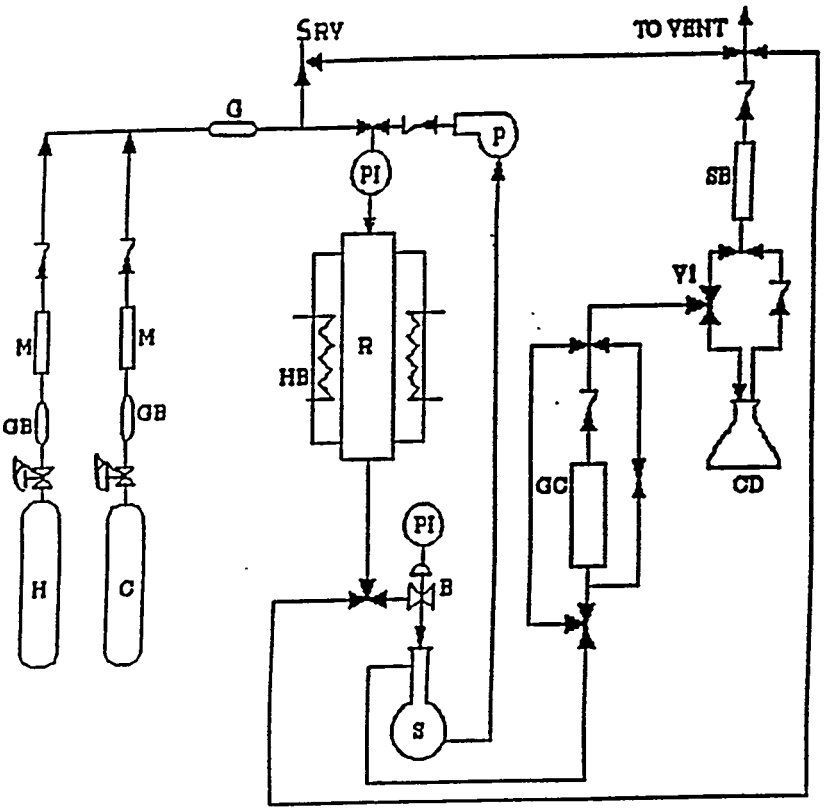

B. Back Pressure Regulator
C. Carbon Oxides Mixture
CD. Condenser
G. Glass Bead Bed
GB. Guard Bed
H. Hydrogen
HB. Heating Block
M. Mass Flow Controller
P. Pump
PI. Pressure Indicator
R. Reactor
RV. Relieve Valve
S. Separator
SB. Soap Bubble Meter
VI. Three Way Valve

Figure 2.4. Schematic diagram of trickle bed reactor system.

1. hydrogen cylinder
2. CO cylinder
3. activated carbon trap
4. activated carbon trap
5. mass flow controller
6. mass flow controller
7. glass beads mixer
8. autoclave reactor
9. recirculation pump
10. back pressure regulator
11. gas-oil separator
12. soap bubble meter

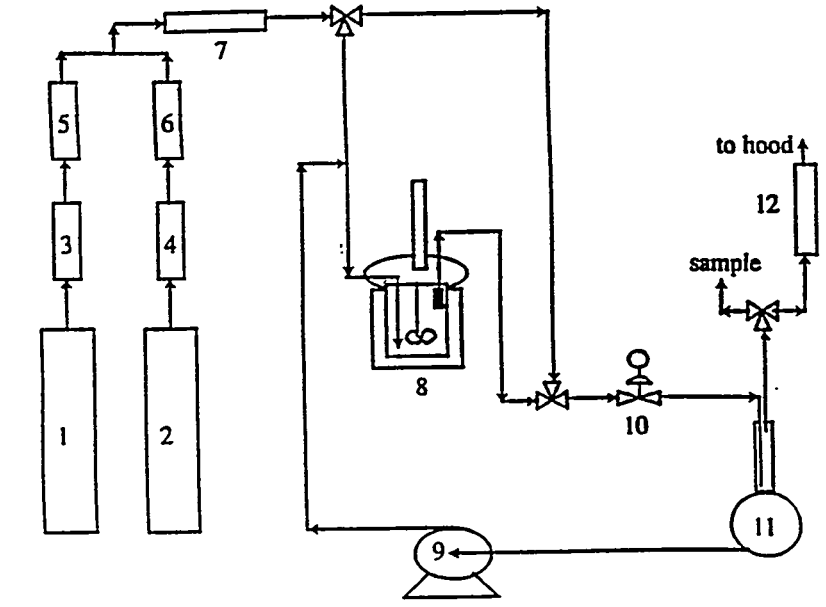

Figure 2.5. Schematic diagram of slurry reactor system.

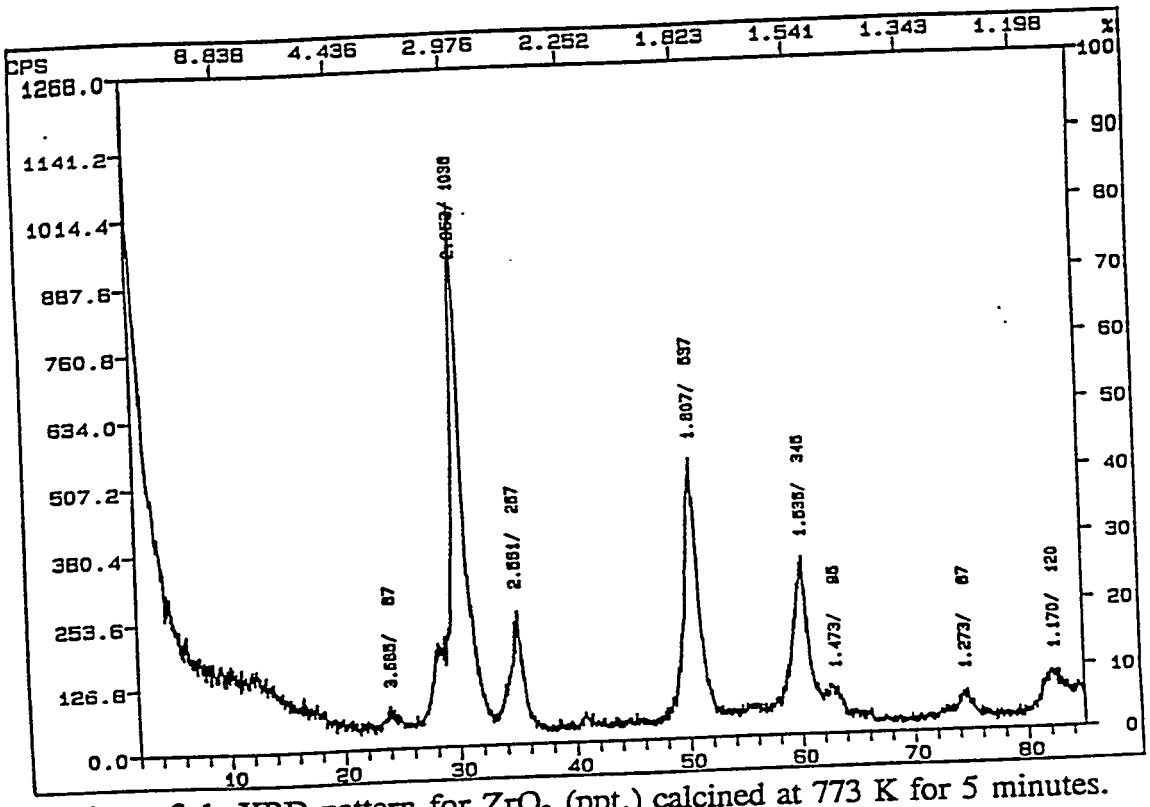

Figure 3.1. XRD pattern for ZrO_2 (ppt.) calcined at 773 K for 5 minutes.

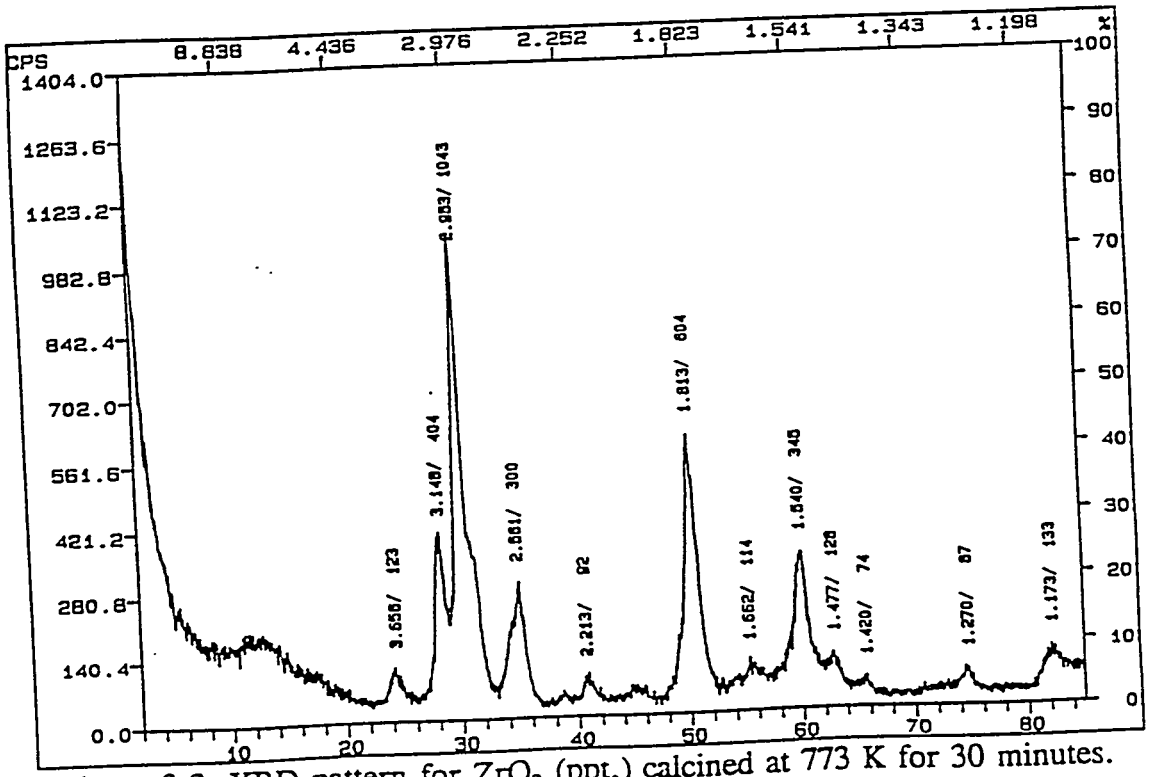

Figure 3.2. XRD pattern for ZrO_2 (ppt.) calcined at 773 K for 30 minutes.

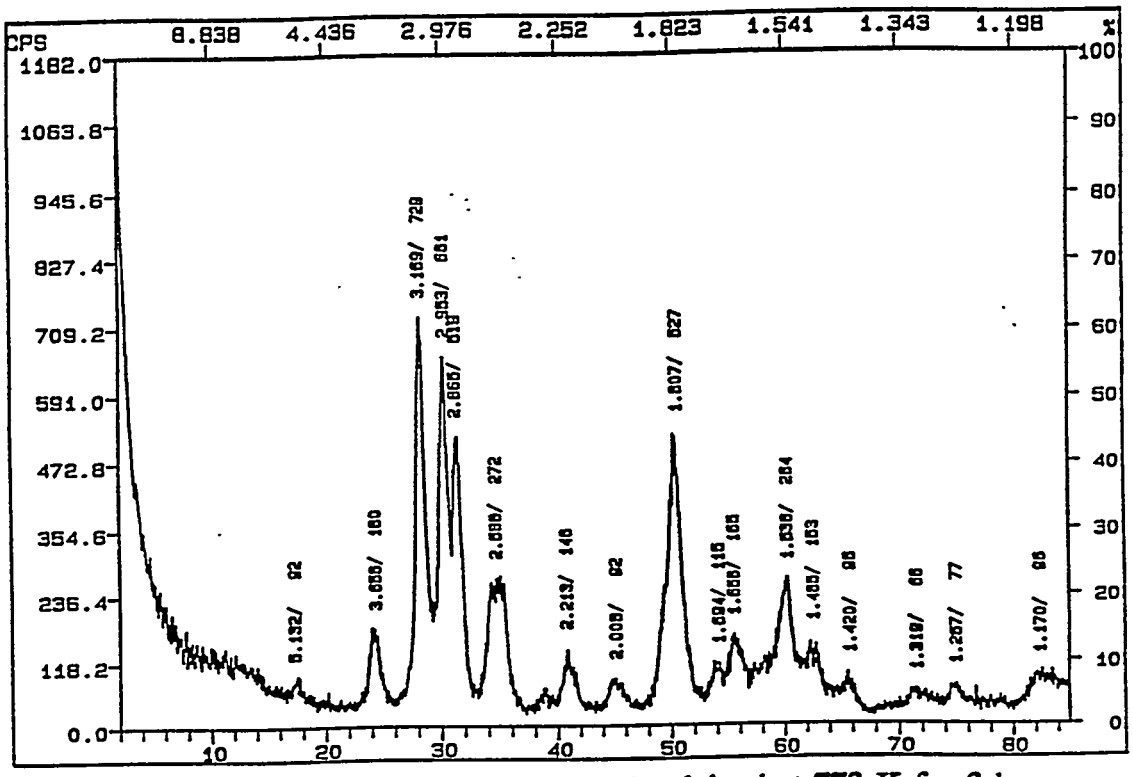

Figure 3.3. XRD pattern for ZrO_2 (ppt.) calcined at 773 K for 3 hours.

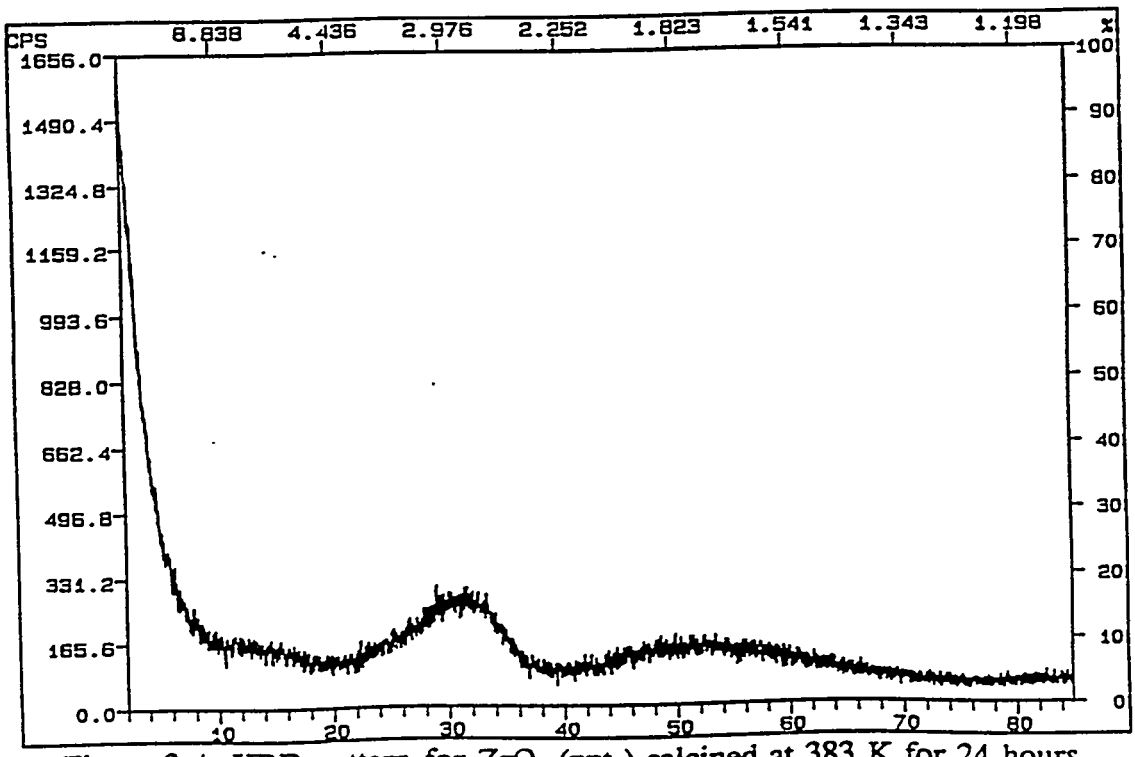

Figure 3.4. XRD pattern for ZrO_2 (ppt.) calcined at 383 K for 24 hours.

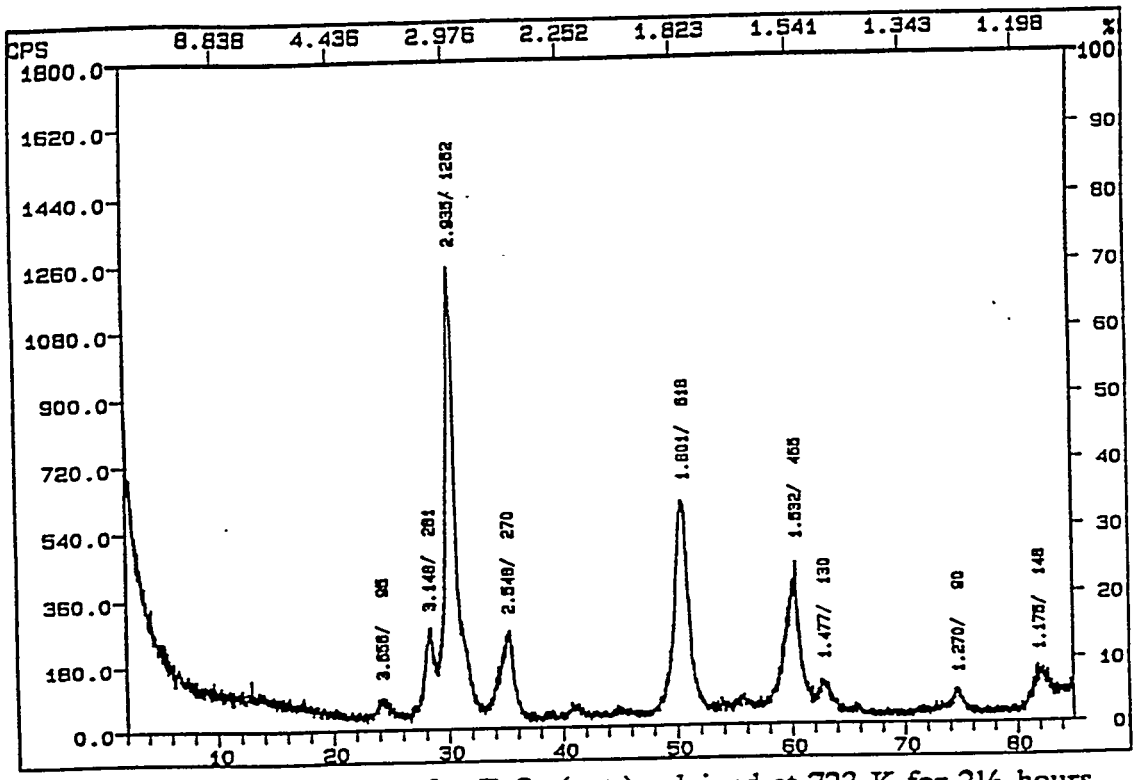

Figure 3.5. XRD pattern for ZrO_2 (ppt.) calcined at 723 K for 2½ hours.

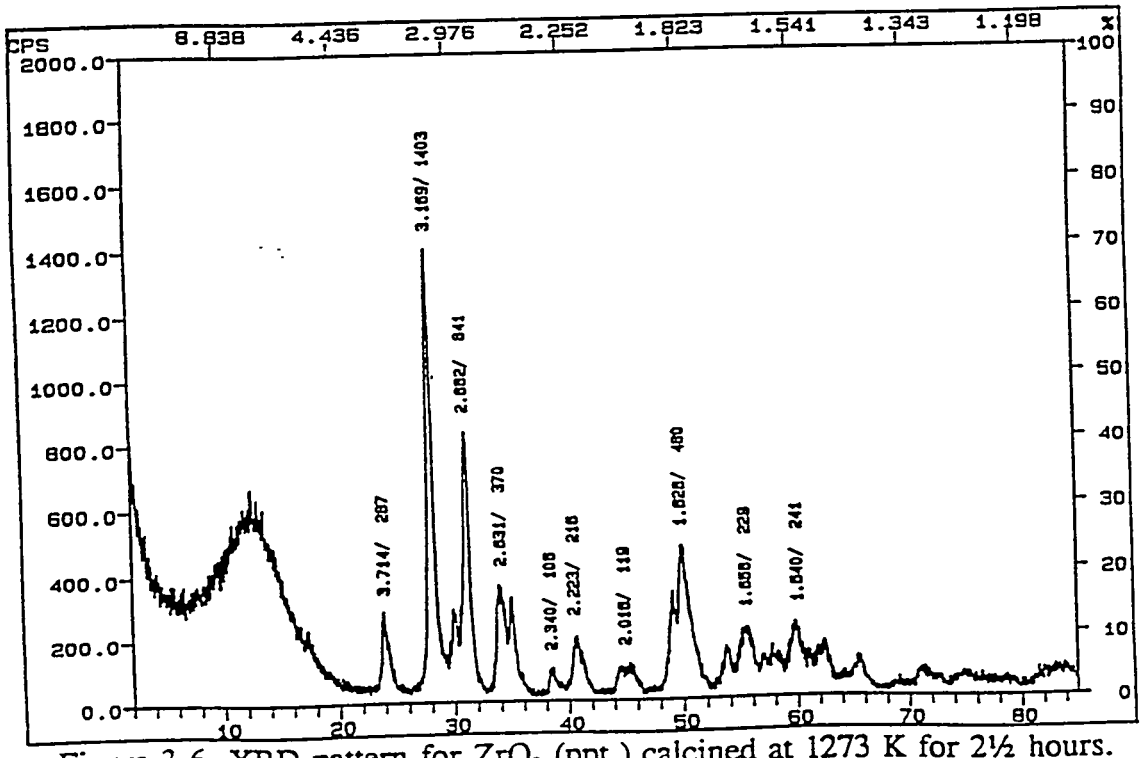

Figure 3.6. XRD pattern for ZrO_2 (ppt.) calcined at 1273 K for 2½ hours.

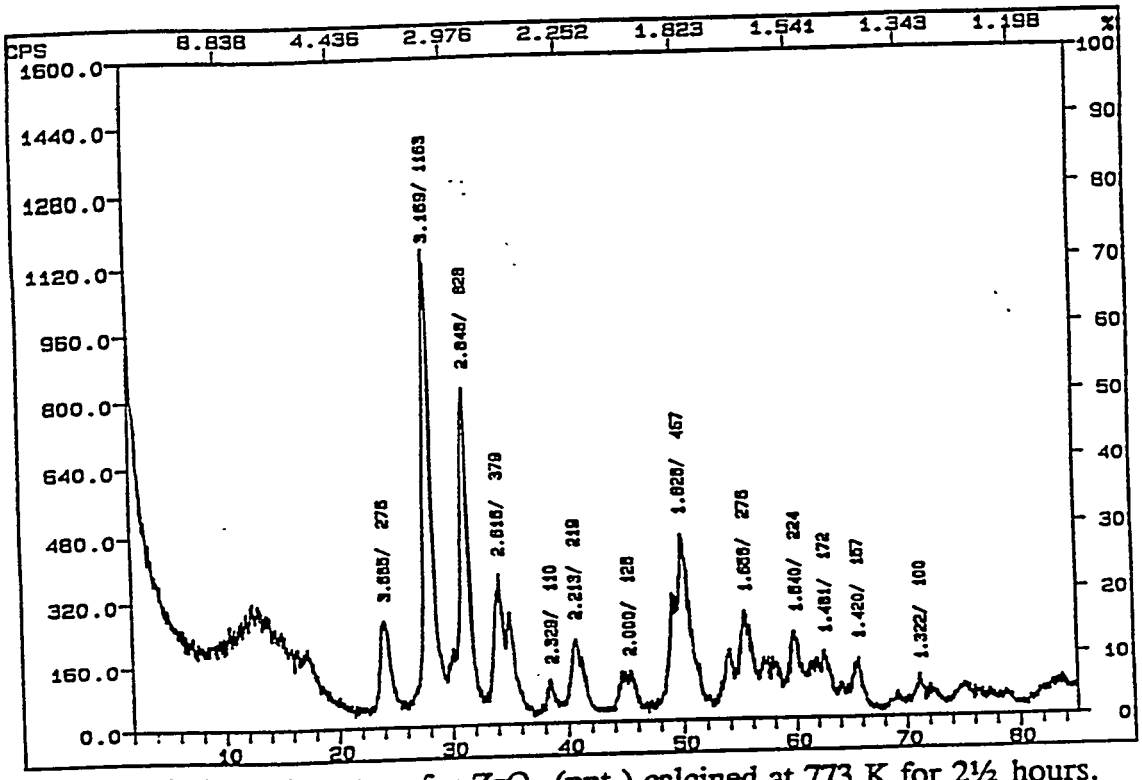

Figure 3.7. XRD pattern for ZrO_2 (ppt.) calcined at 773 K for 2½ hours.

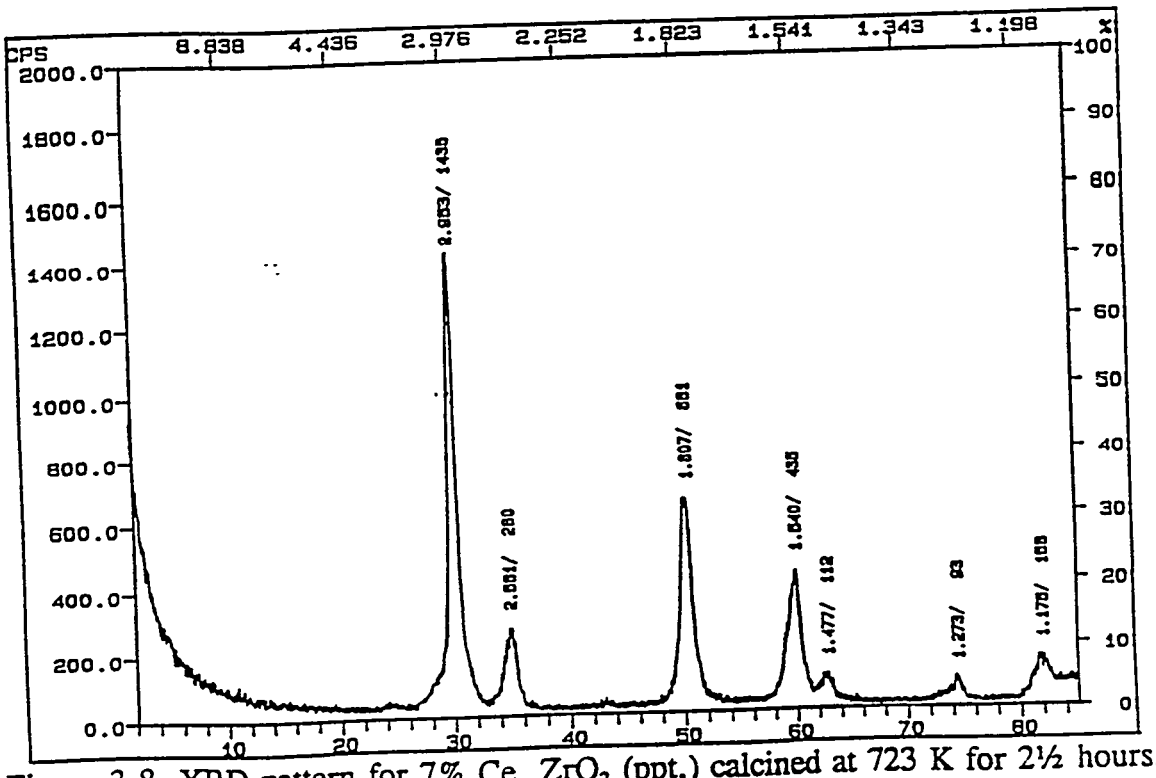

Figure 3.8. XRD pattern for 7% Ce, ZrO_2 (ppt.) calcined at 723 K for 2½ hours.

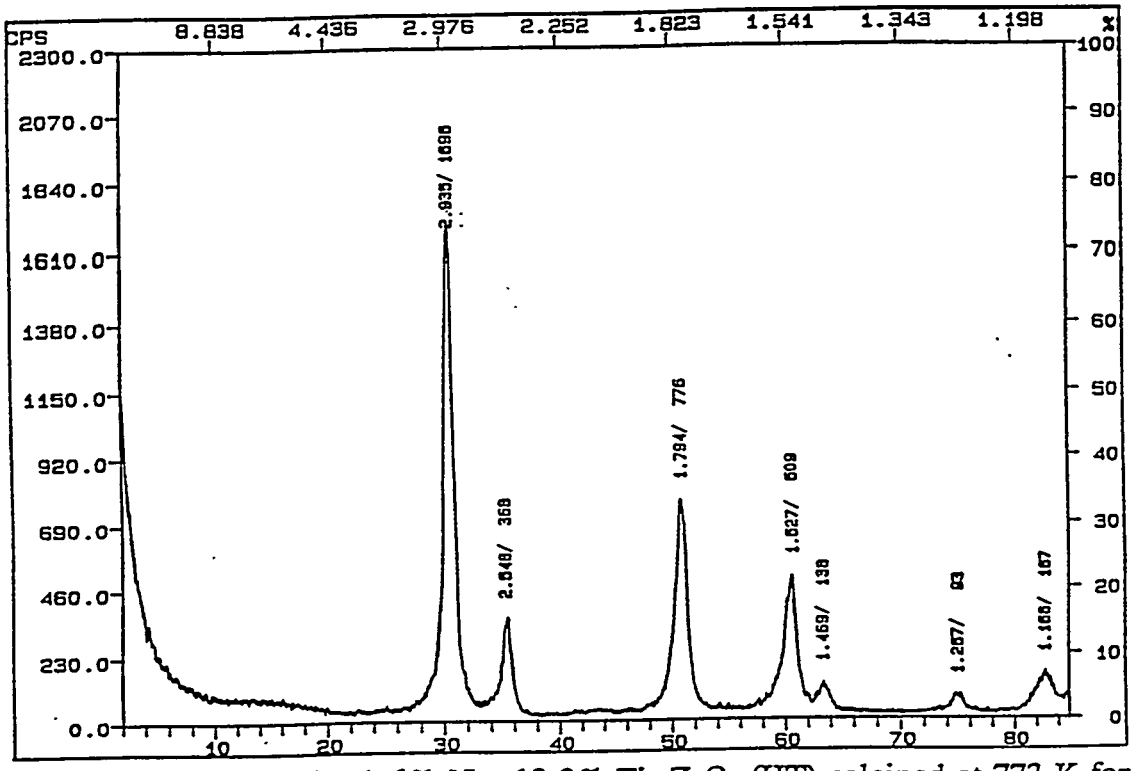

Figure 3.9. XRD pattern for 1.6% Na, 10.3% Ti, ZrO_2 (HT) calcined at 773 K for 2½ hours.

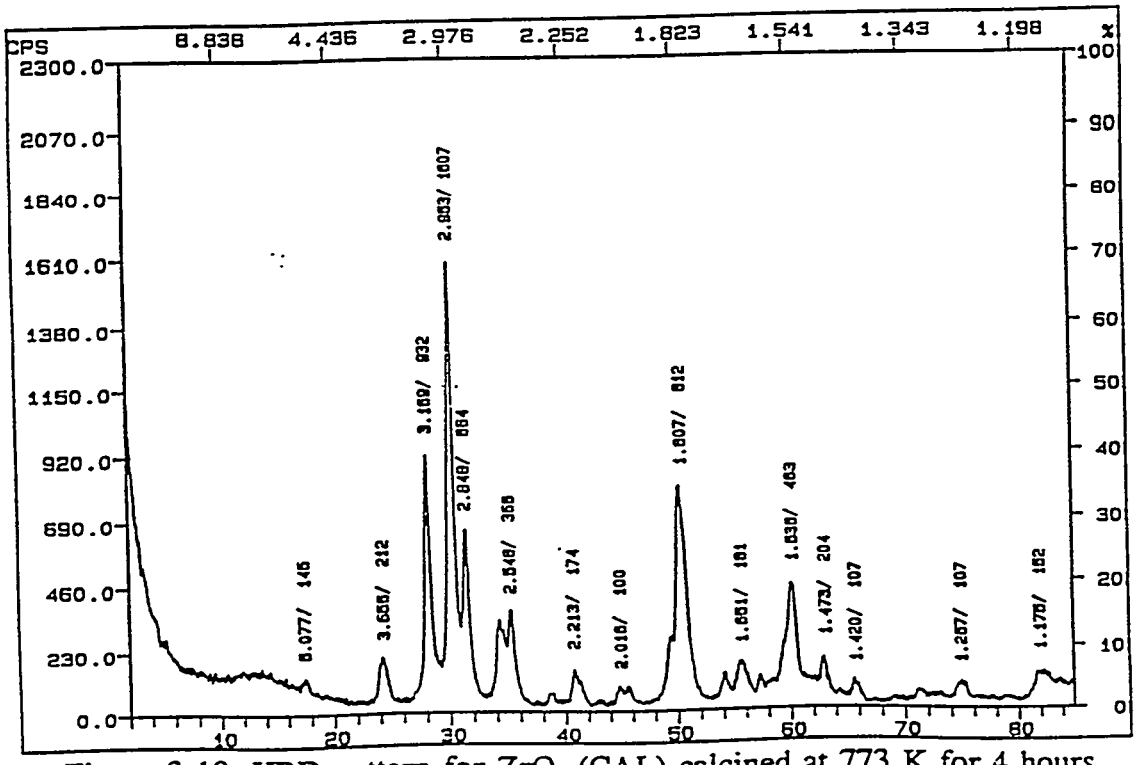

Figure 3.10. XRD pattern for ZrO_2 (CAL) calcined at 773 K for 4 hours.

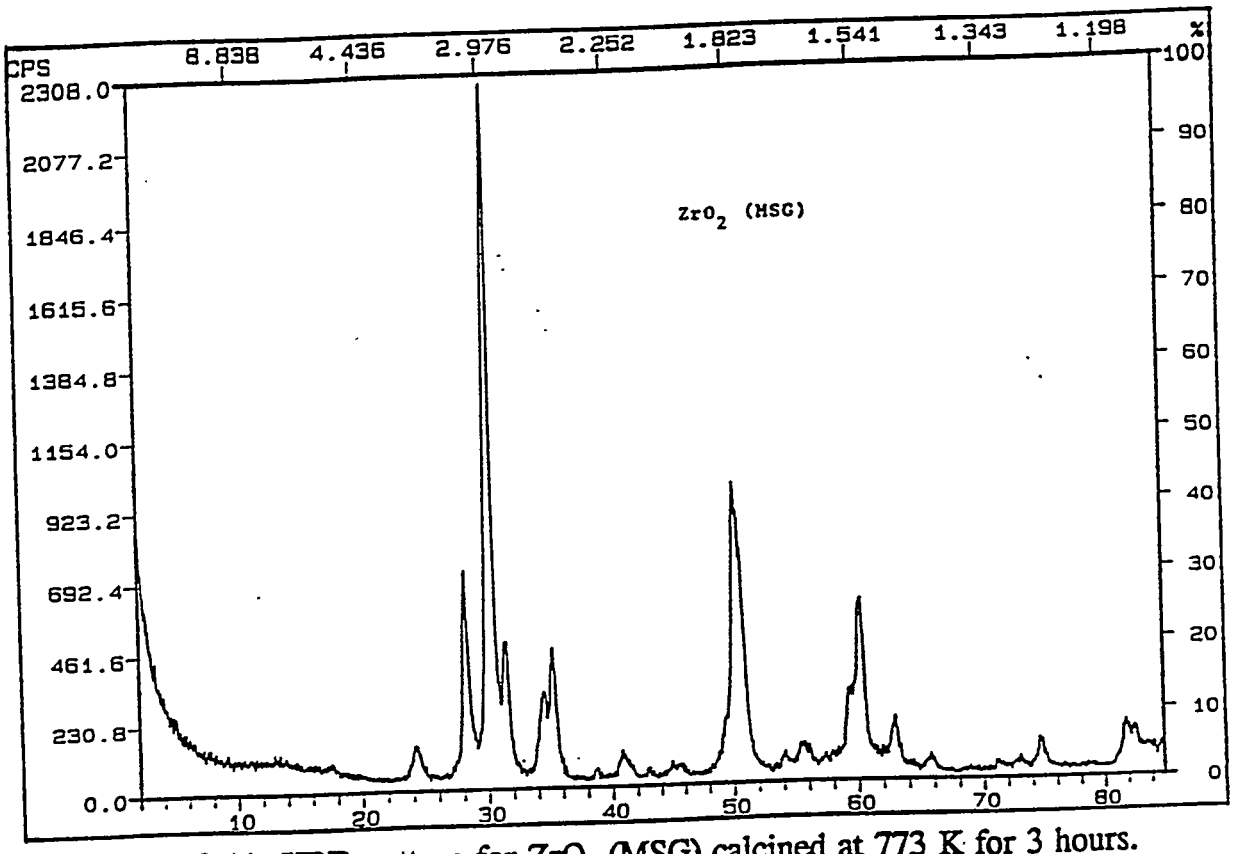

Figure 3.11. XRD pattern for ZrO_2 (MSG) calcined at 773 K for 3 hours.

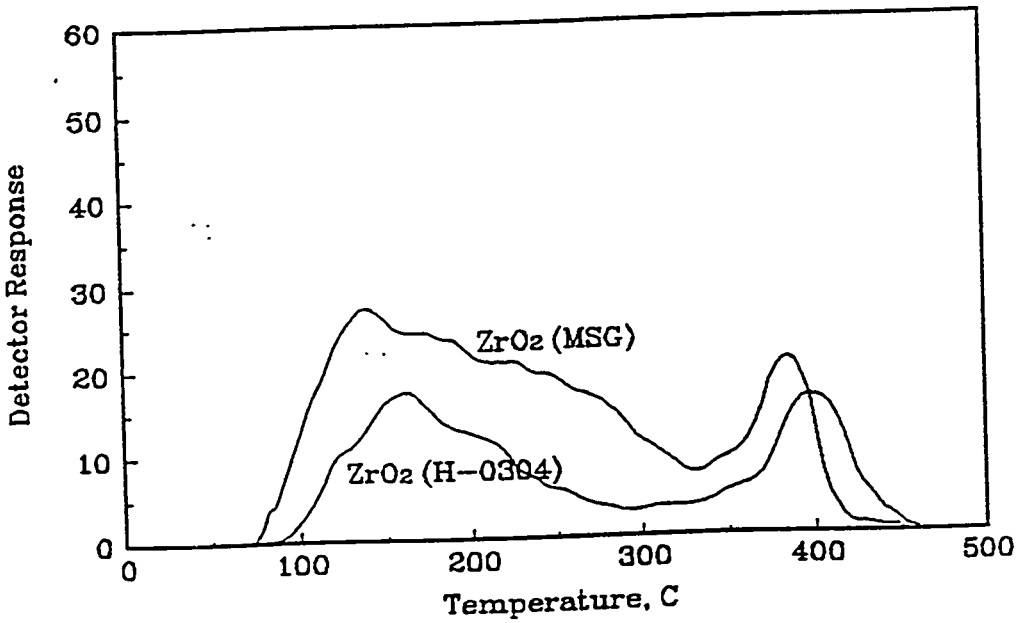

Figure 3.12. A comparison of basicity for catalysts prepared by different methods. TPD of CO_2, 0.2 g catalyst. ZrO_2 (MSG) has more basic sites.

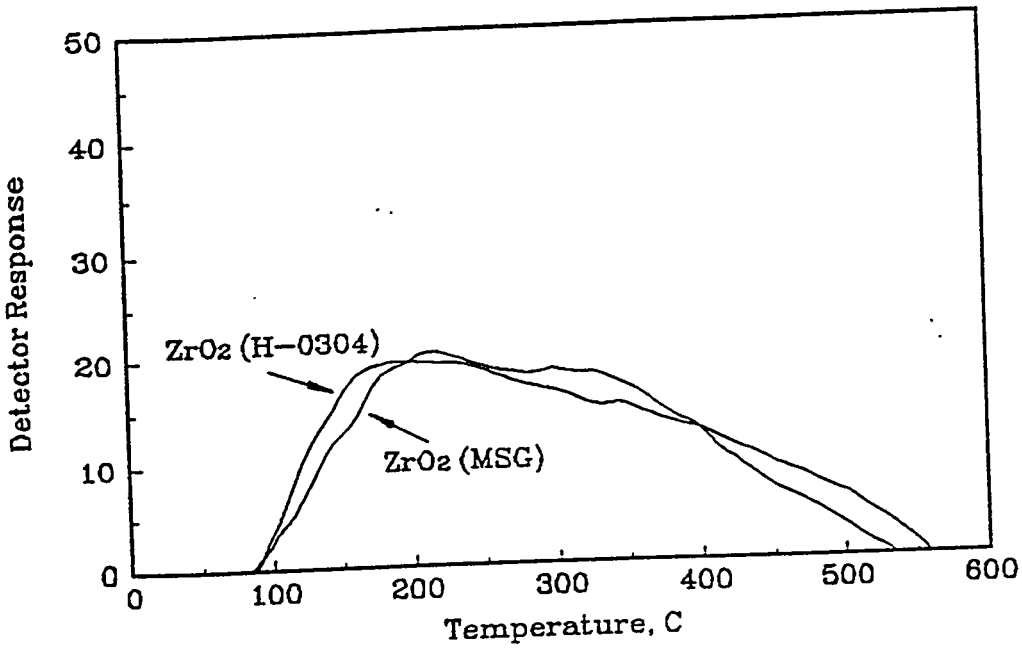

Figure 3.13. A comparison of acidity for catalysts prepared by different methods. TPD of NH_3, 0.2 g catalyst. Catalysts have similar acidity.

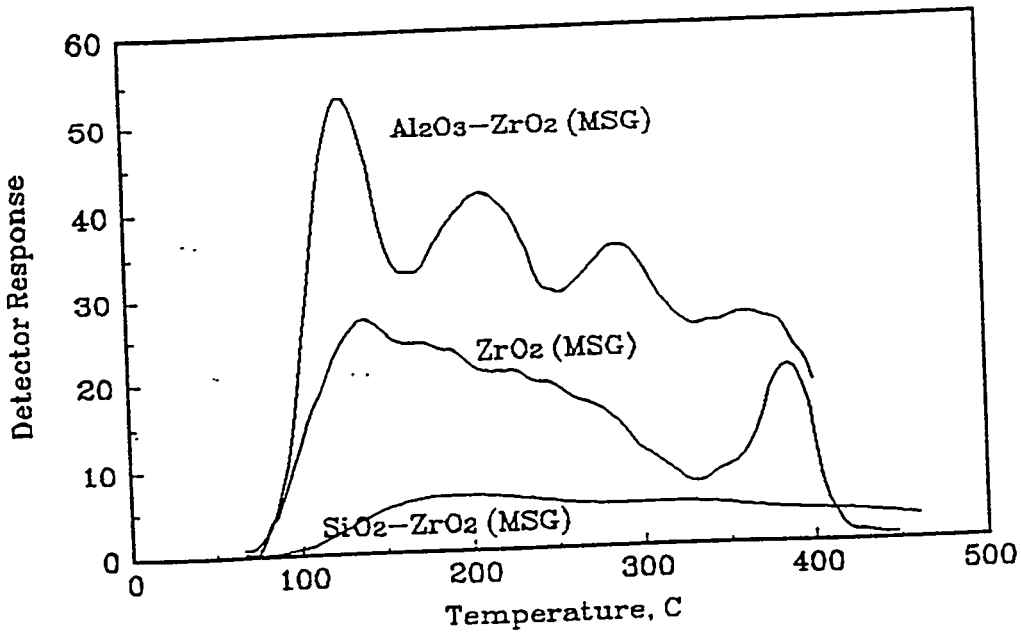

Figure 3.14. Basicity of the catalysts prepared by the modified sol gel method. TPD of CO_2, 0.2 g catalyst.

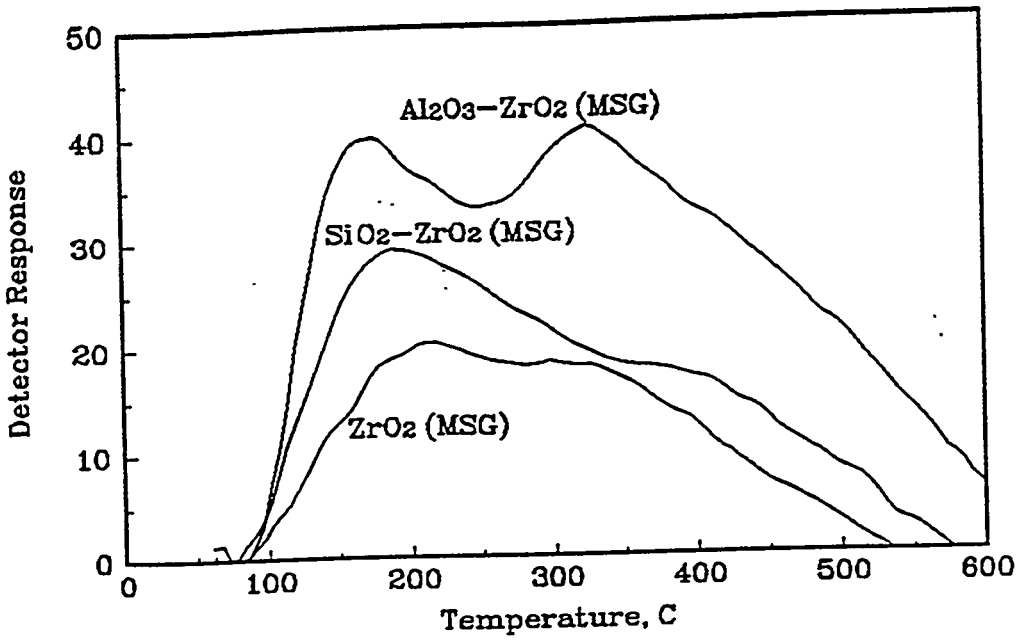

Figure 3.15. Acidity of the catalysts prepared by the modified sol gel method. TPD of NH_3, 0.2 g catalyst.

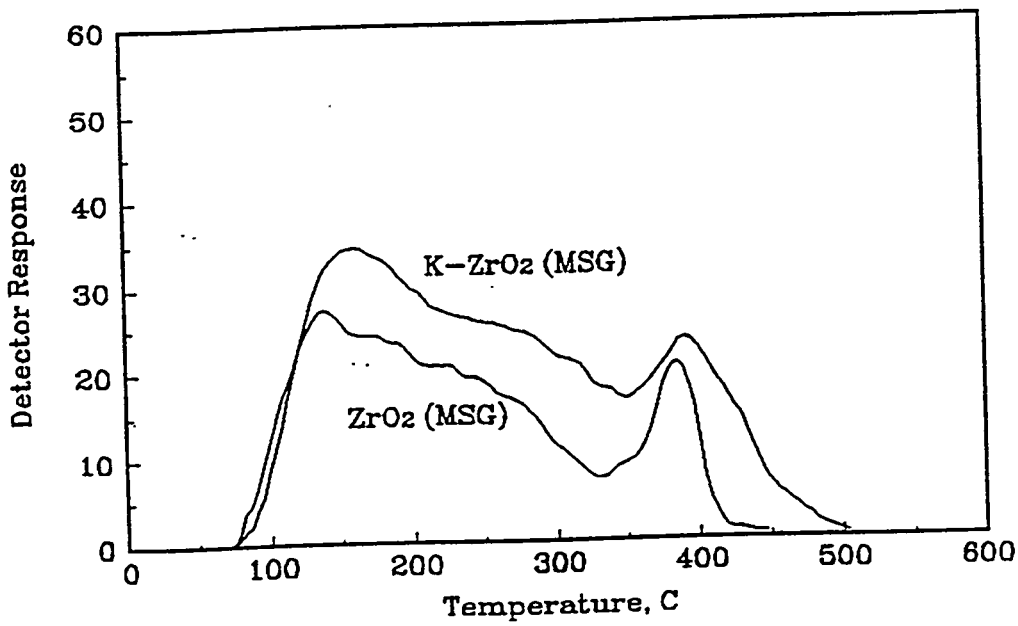

Figure 3.16. Modification of basicity by potassium. TPD of CO_2, 0.2 g catalyst.

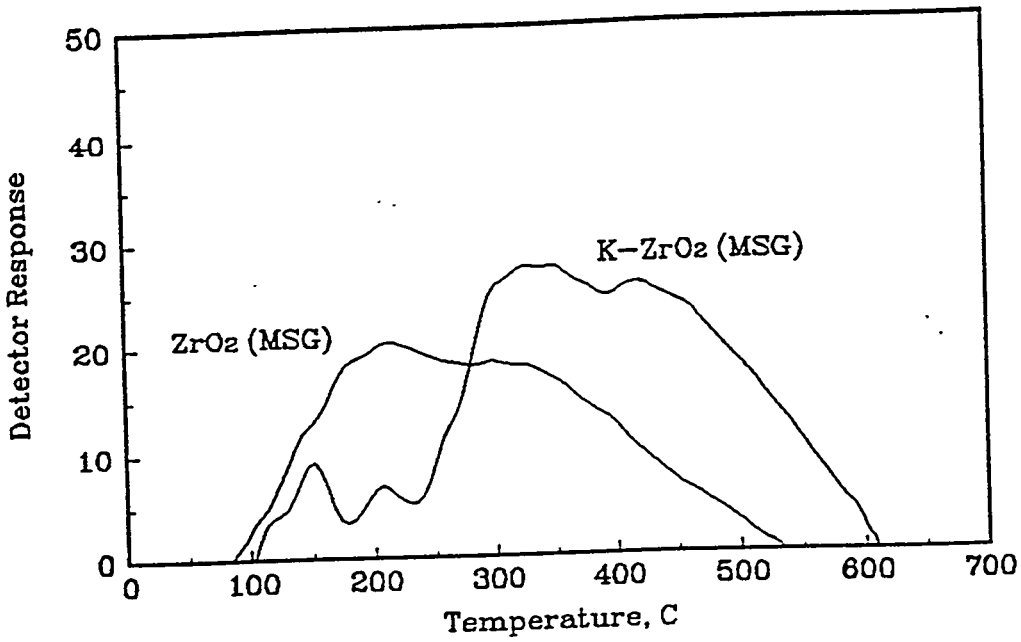

Figure 3.17. Modification of acidity by potassium. TPD of NH_3, 0.2 g catalyst.

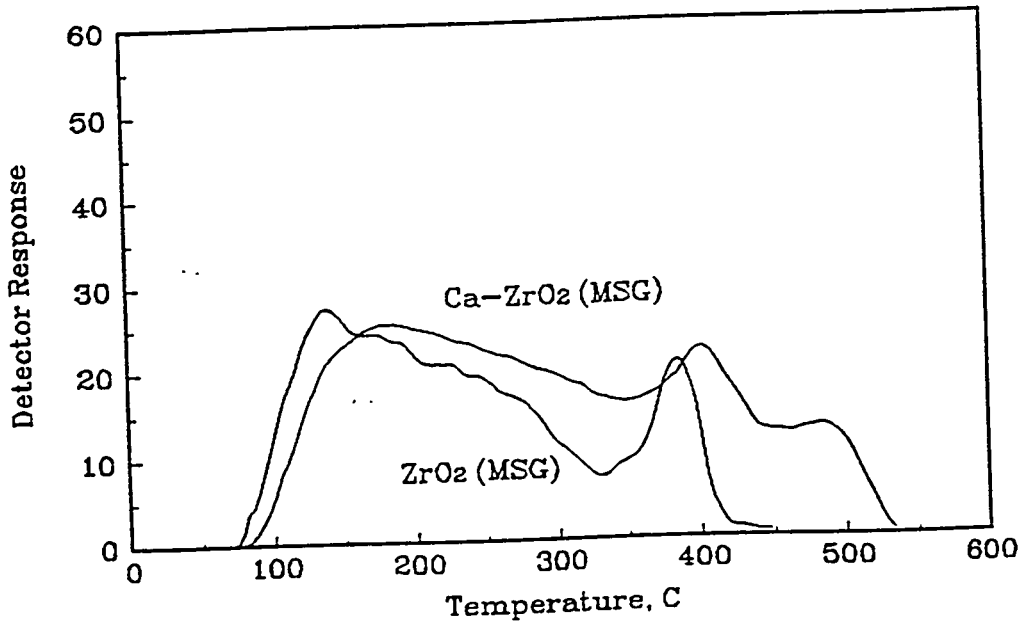

Figure 3.18. Modification of basicity by calcium. TPD of CO_2, 0.2 g catalyst.

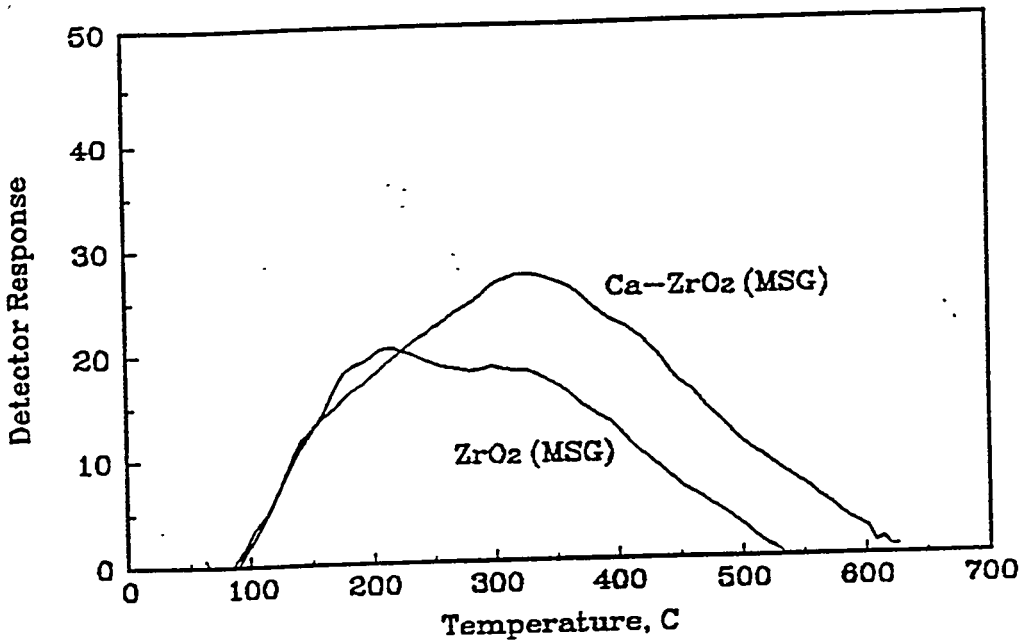

Figure 3.19. Modification of acidity by calcium. TPD of NH_3, 0.2 g catalyst.

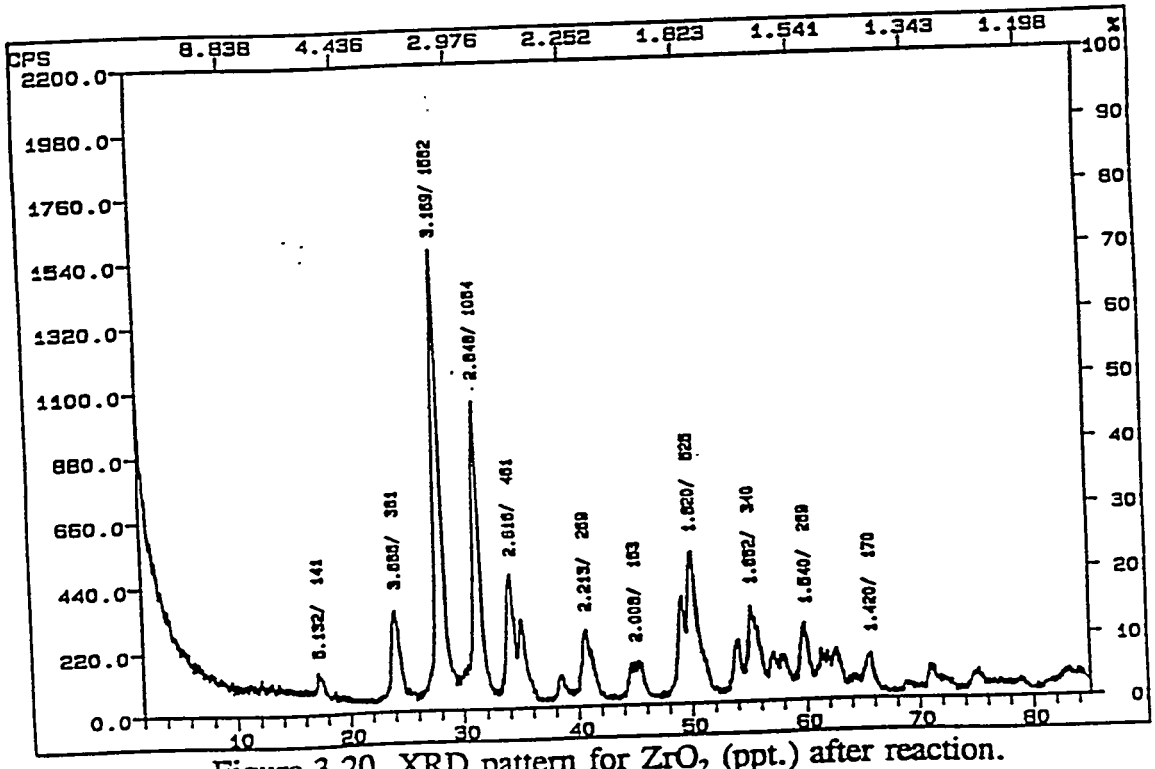

Figure 3.20. XRD pattern for ZrO_2 (ppt.) after reaction.

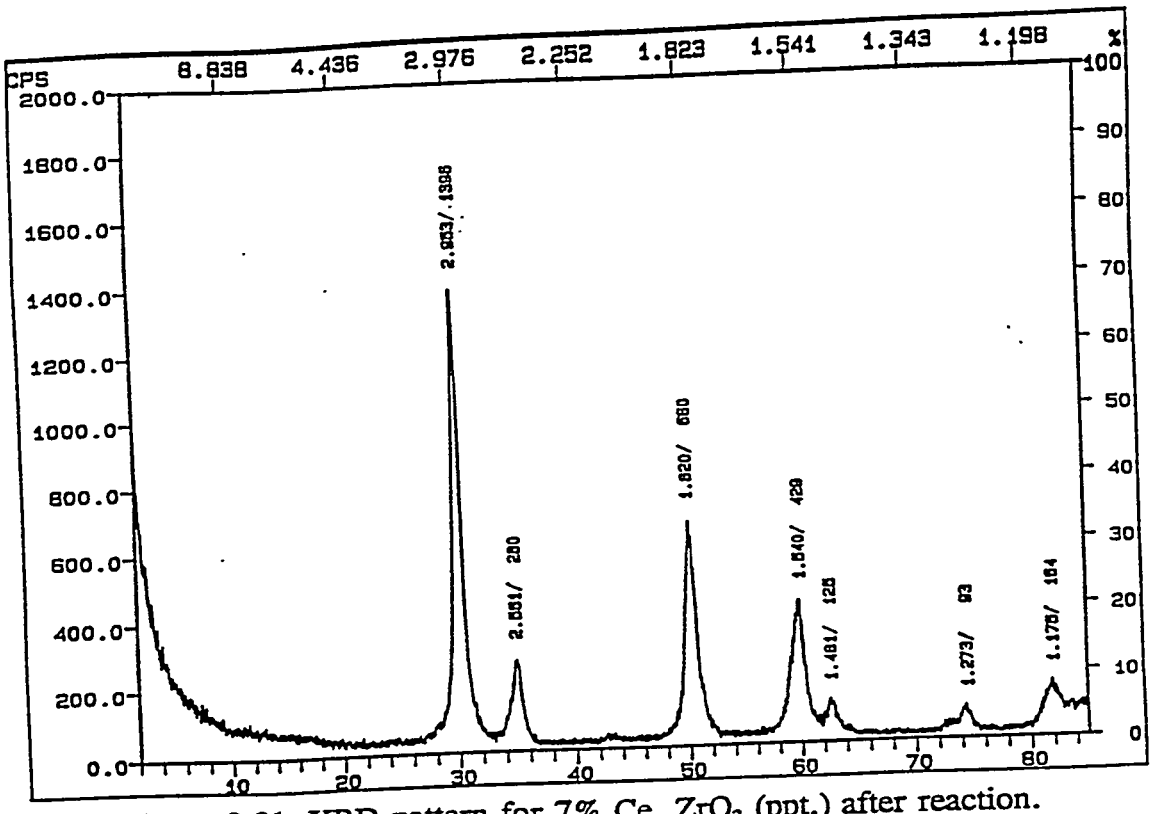

Figure 3.21. XRD pattern for 7% Ce, ZrO_2 (ppt.) after reaction.

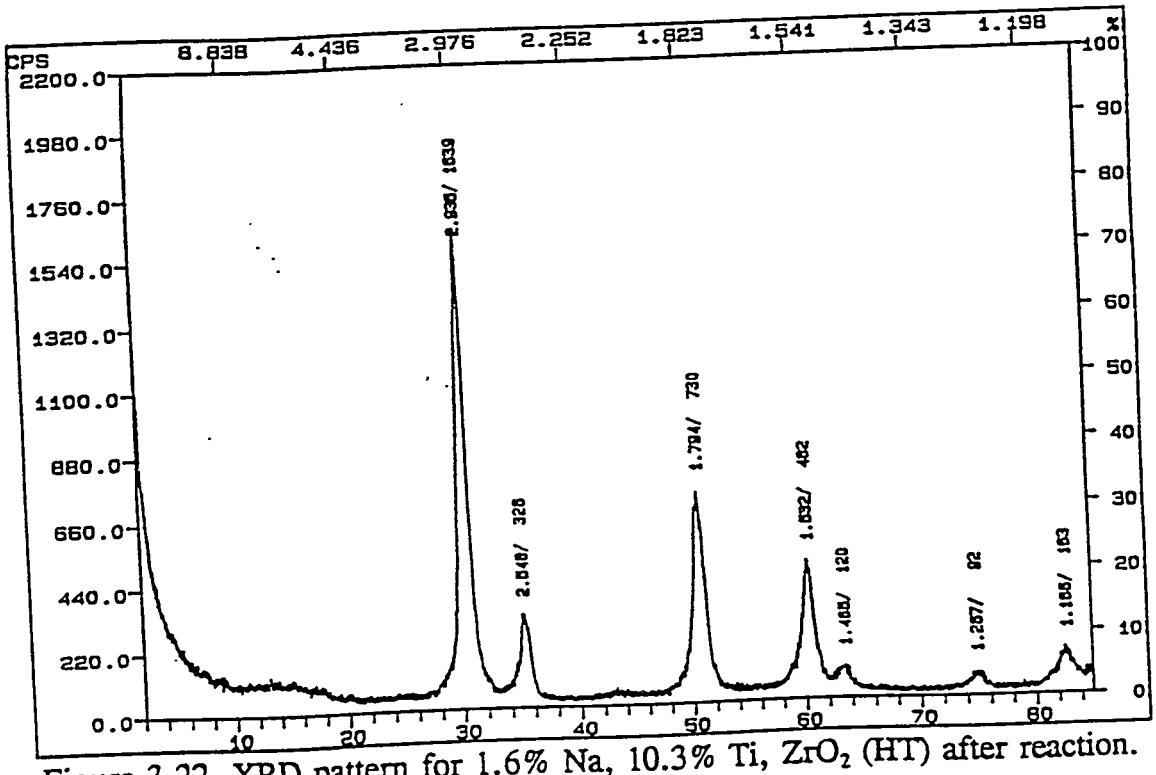

Figure 3.22. XRD pattern for 1.6% Na, 10.3% Ti, ZrO_2 (HT) after reaction.

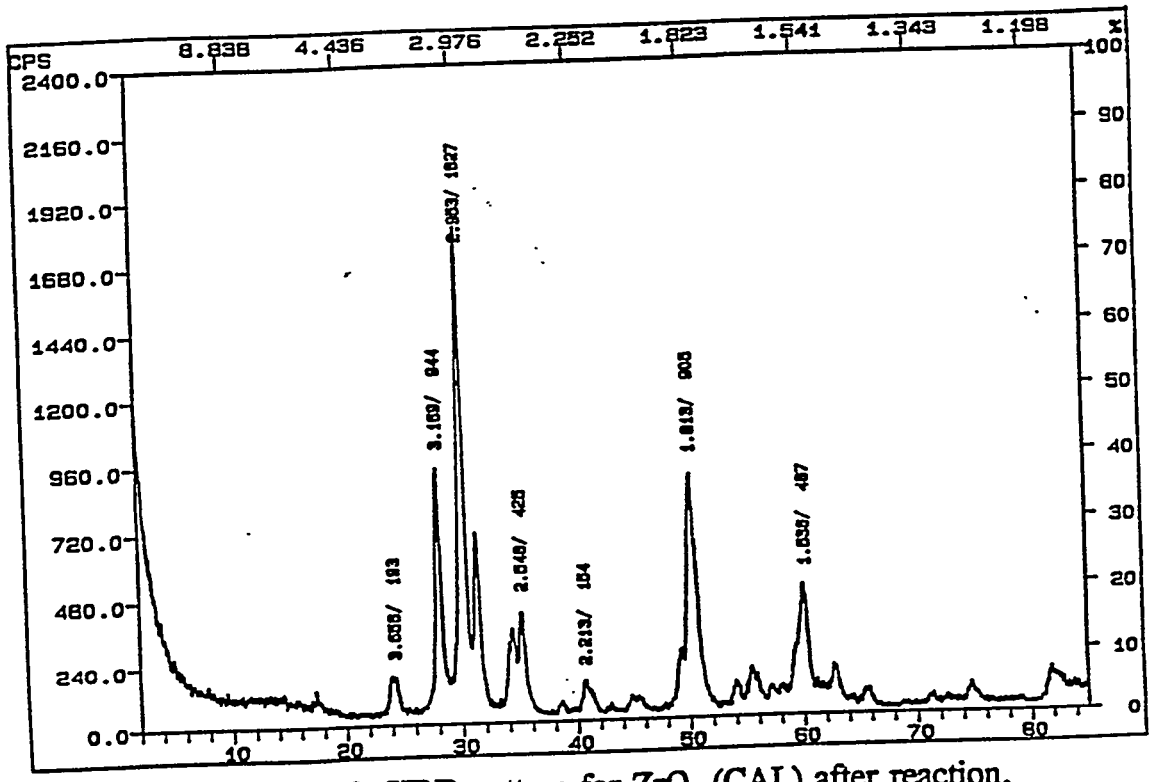

Figure 3.23. XRD pattern for ZrO_2 (CAL) after reaction.

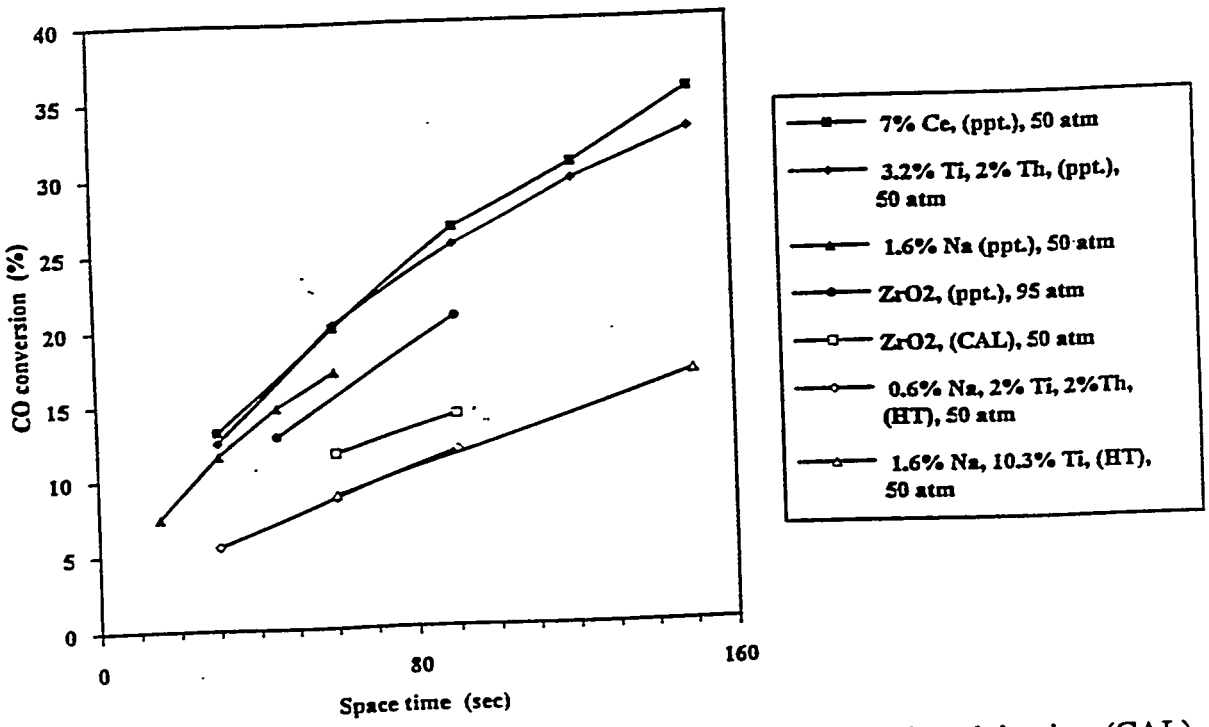

Figure 3.24. Comparison of catalytic activity for precipitated (ppt.), calcination (CAL), and hydrothermally (HT) prepared zirconias at 673 K and 1/1 CO/H_2 ratio.

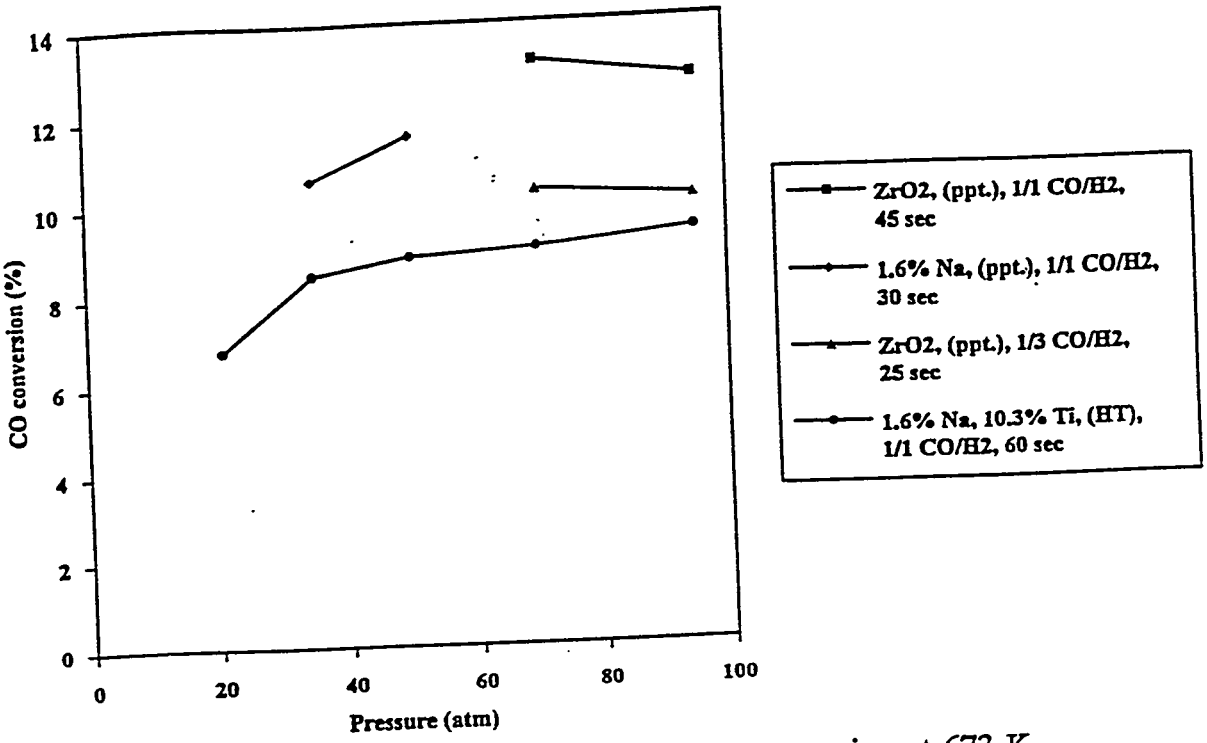

Figure 3.25. Effect of pressure on CO conversion at 673 K.

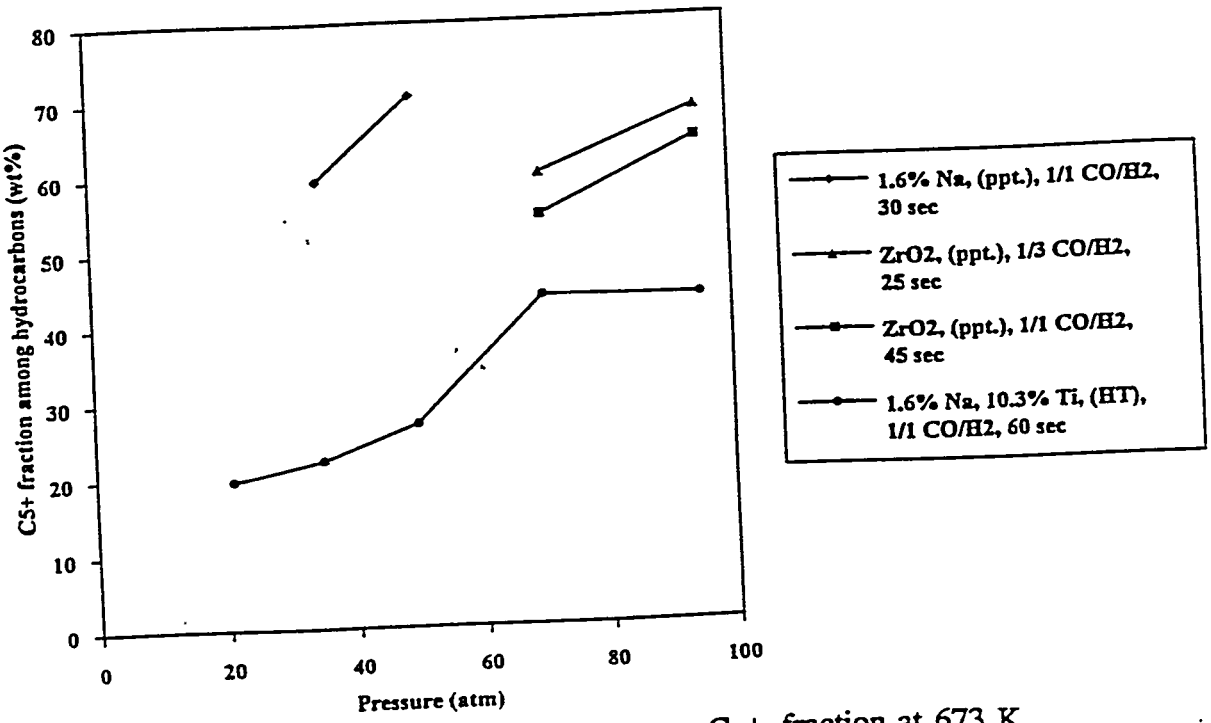

Figure 3.26. Effect of pressure on C_5+ fraction at 673 K.

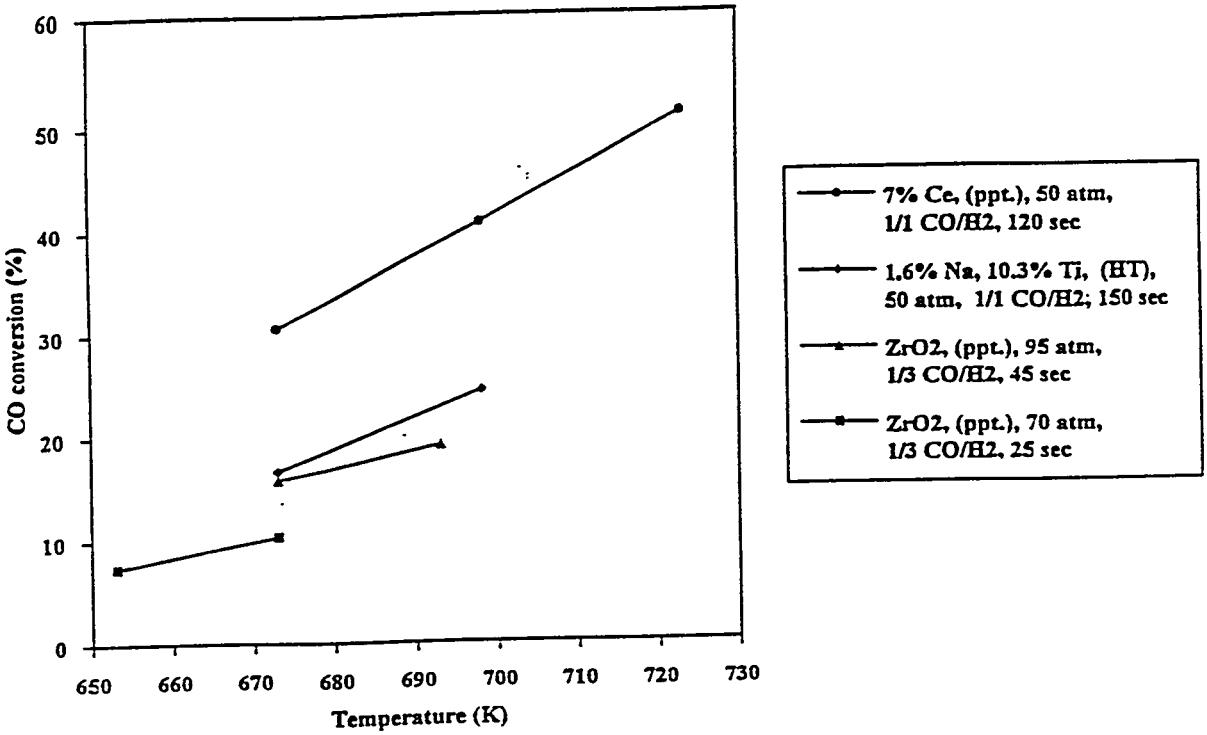

Figure 3.27. Effect of temperature on CO conversion.

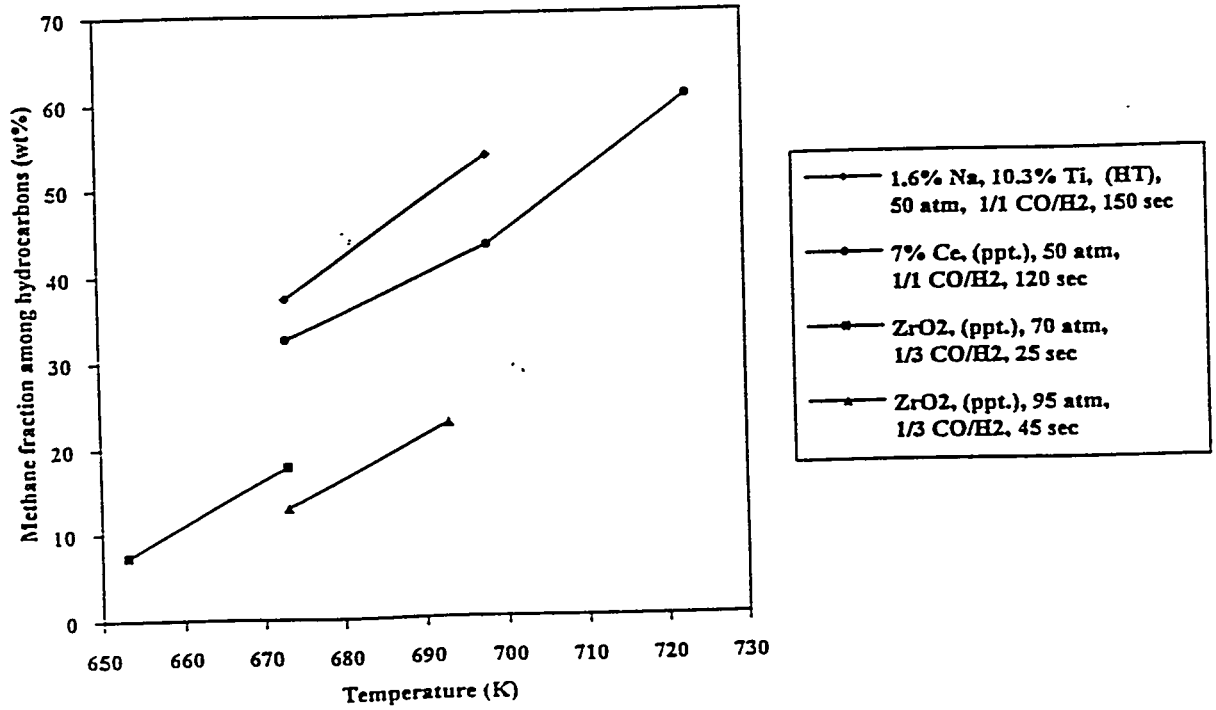

Figure 3.28. Effect of temperature on methane fraction.

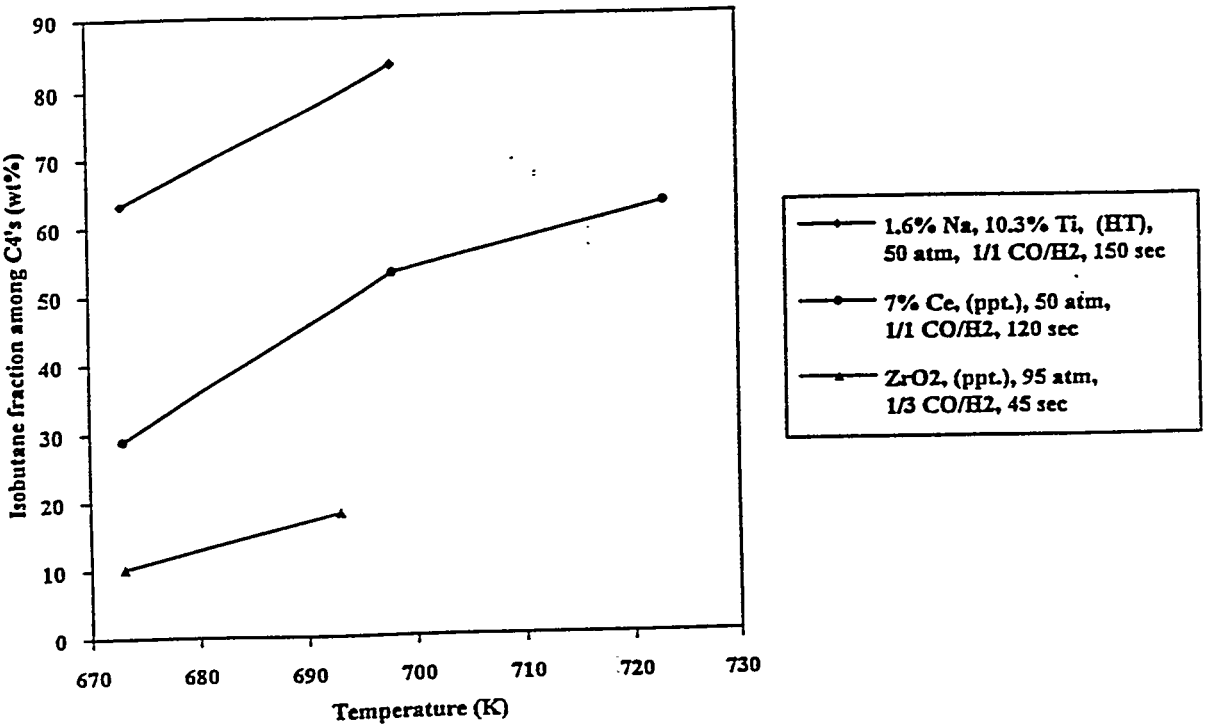

Figure 3.29. Effect of temperature on isobutane fraction among C_4's.

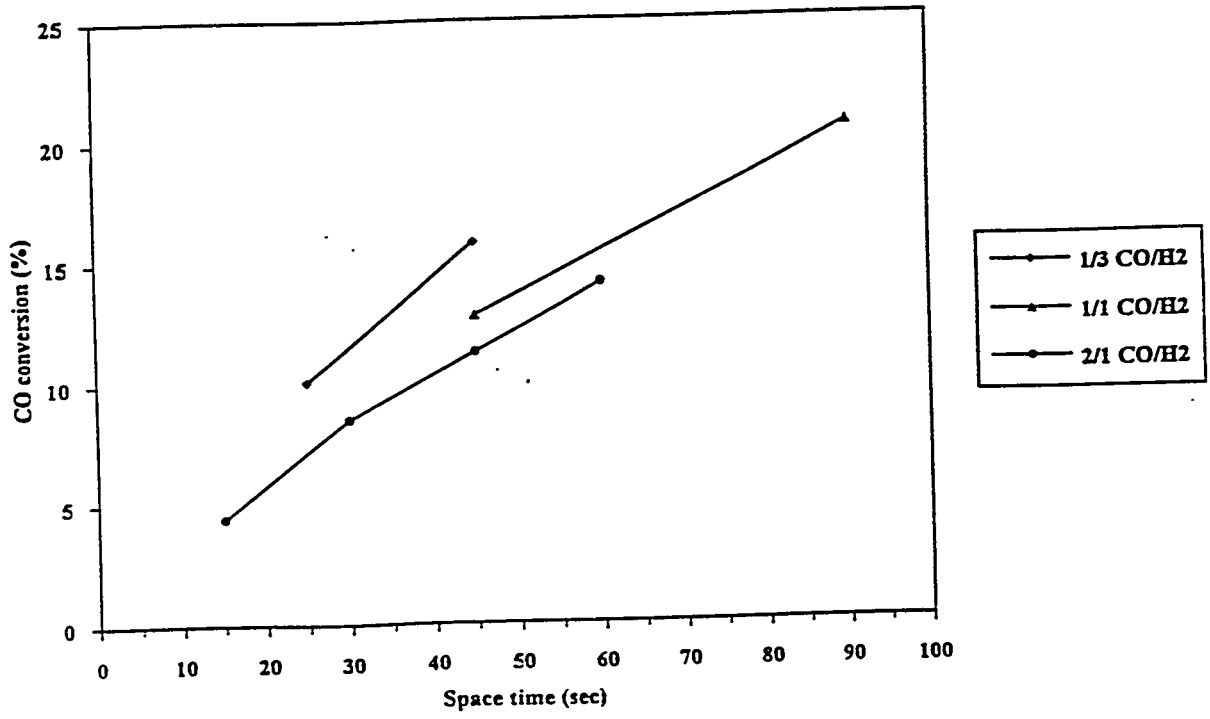

Figure 3.30. Effect of CO/H_2 ratio on CO conversion at 673 K and 95 atm over ZrO_2 (ppt.).

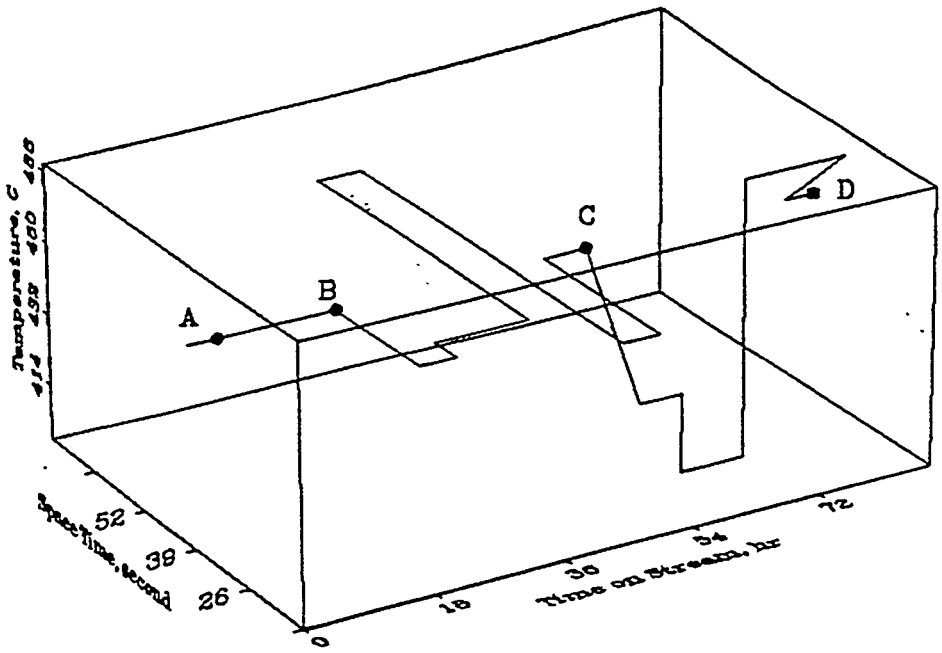

Figure 3.31. Procedure of the study of time on stream.

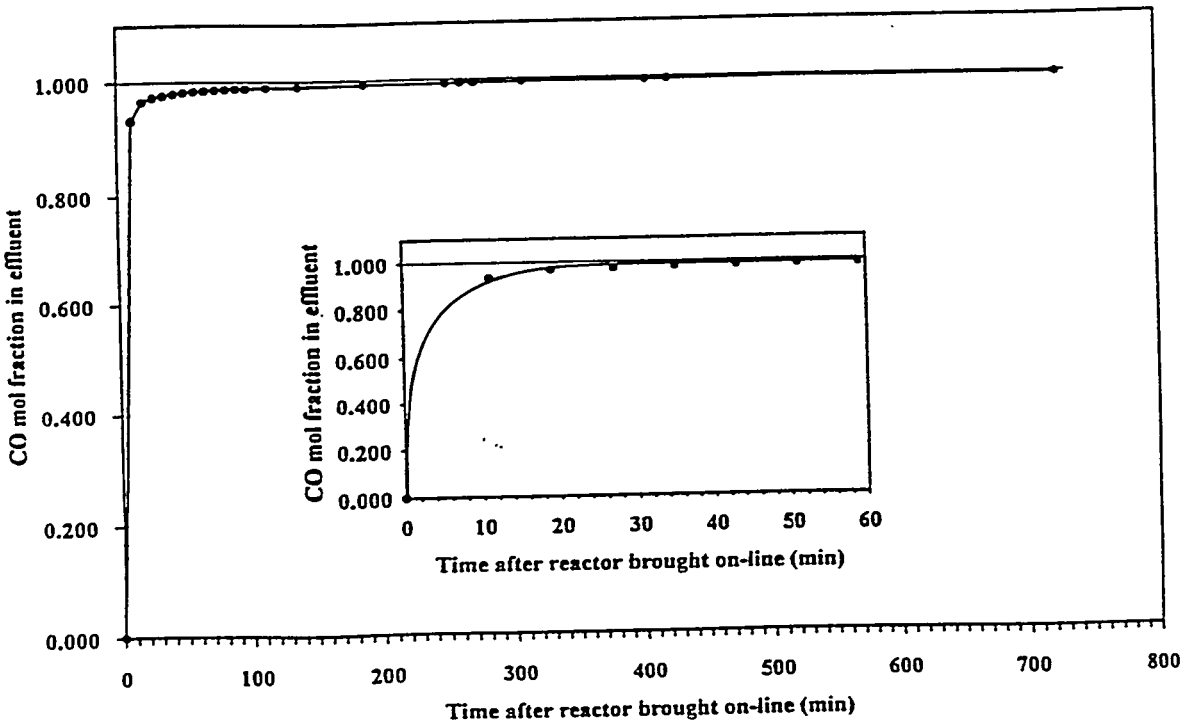

Figure 3.32. Breakthrough curve for CO over 7% Ce-ZrO_2 at 673 K, 25 atm, and 90 second space time.

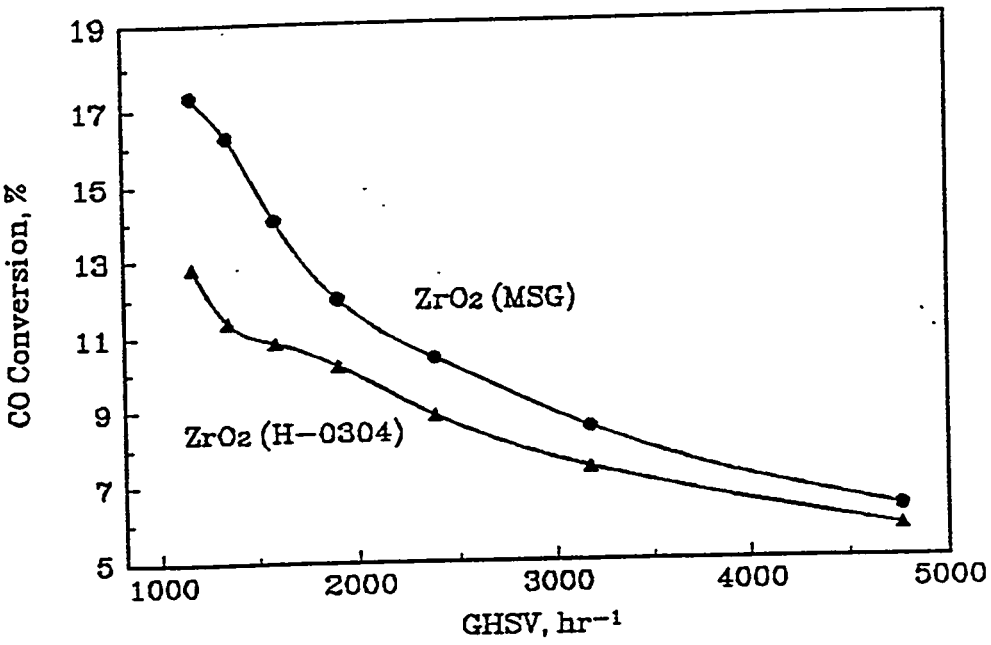

Figure 3.33. Activities of ZrO_2 (MSG) and ZrO_2 (H-0304) at 723 K, 70 atm, and 1/1 CO/H_2 ratio.

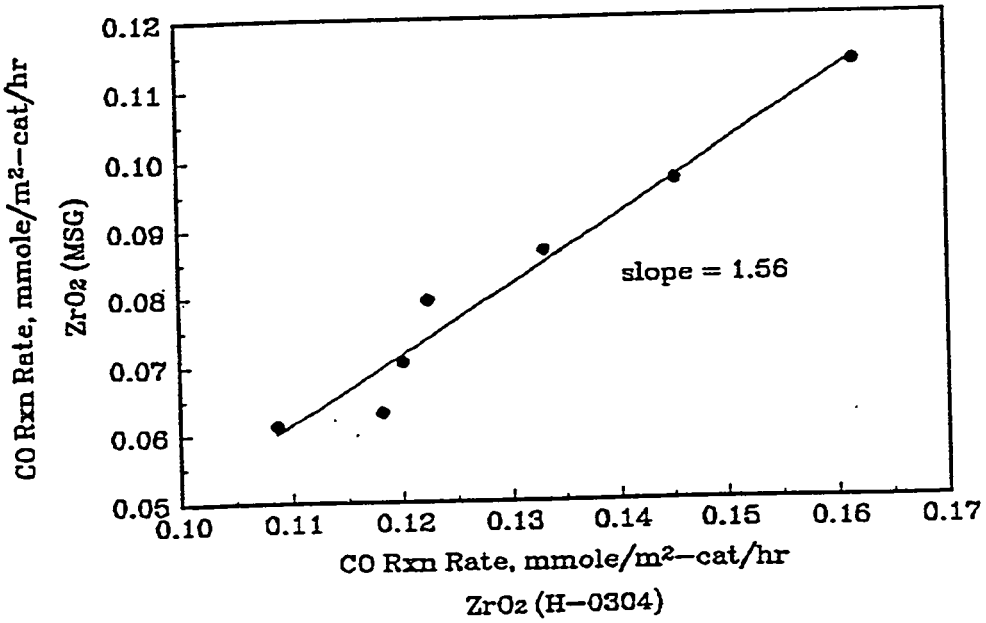

Figure 3.34. Reaction rates of CO over ZrO_2 (H-0304) and ZrO_2 (MSG) at 723 K, 70 atm, and 1/1 CO/H_2 ratio. CO reaction rates were calculated from Figure 3.33 and each scatter point corresponds to a space velocity.

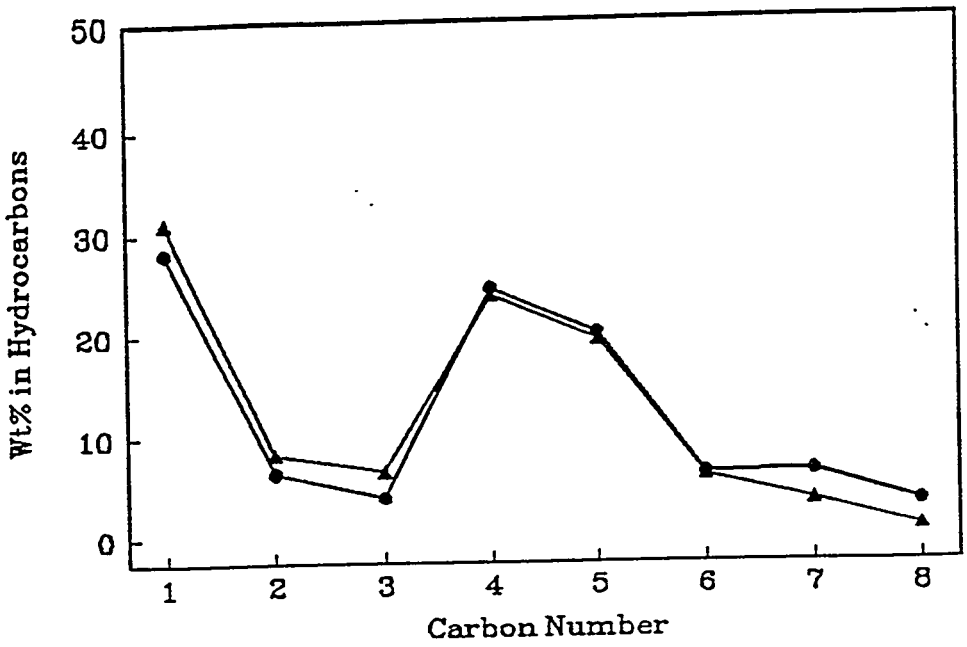

Figure 3.35. Distribution of hydrocarbons at 723 K, 70 atm, 1/1 CO/H_2 ratio, and CO conversion 11 to 12%: ▲-ZrO_2 (H-0304); ●-ZrO_2 (MSG).

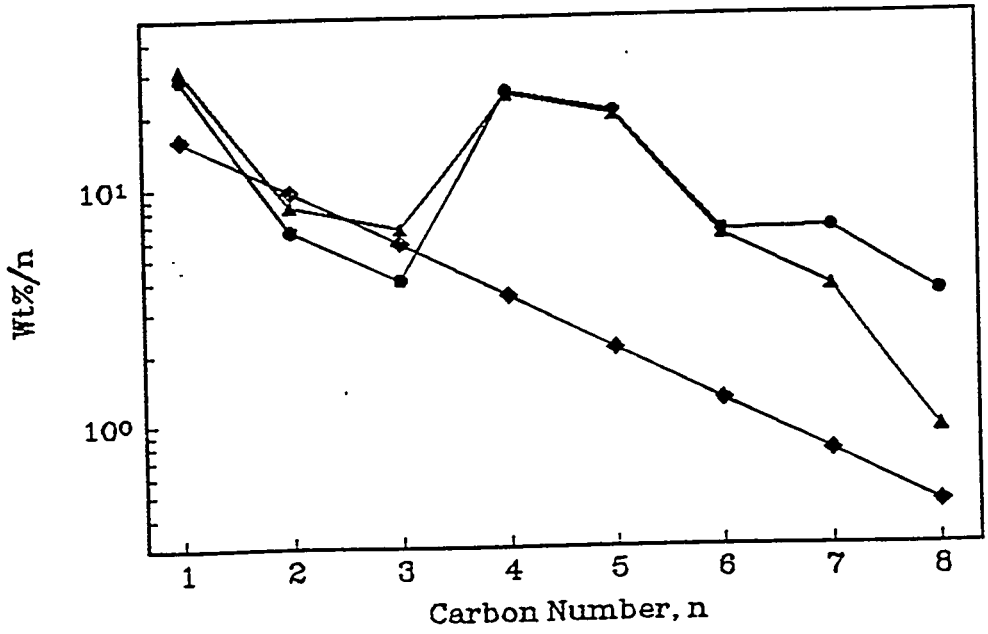

Figure 3.36. The Anderson-Schulz-Flory plots of hydrocarbon distributions for isosynthesis and Fischer-Tropsch synthesis. Isosynthesis: ▲-ZrO_2 (H-0304), ●-ZrO_2 (MSG); F-T synthesis: ◆-adapted from Dry (27).

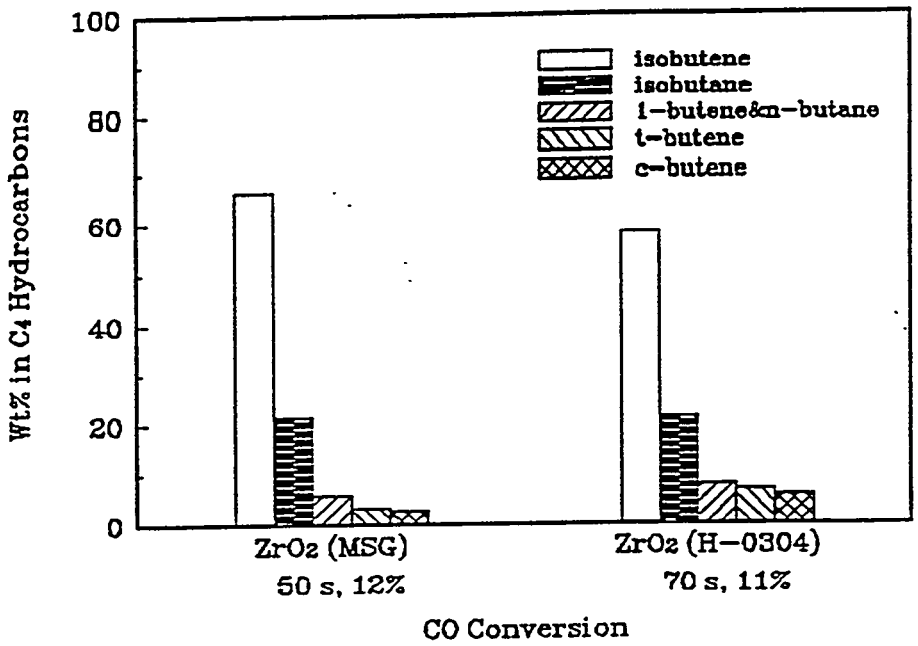

Figure 3.37. Distribution of C_4 hydrocarbons over ZrO_2 (MSG) and ZrO_2 (H-0304) at 723 K, 70 atm, and 1/1 CO/H_2 ratio.

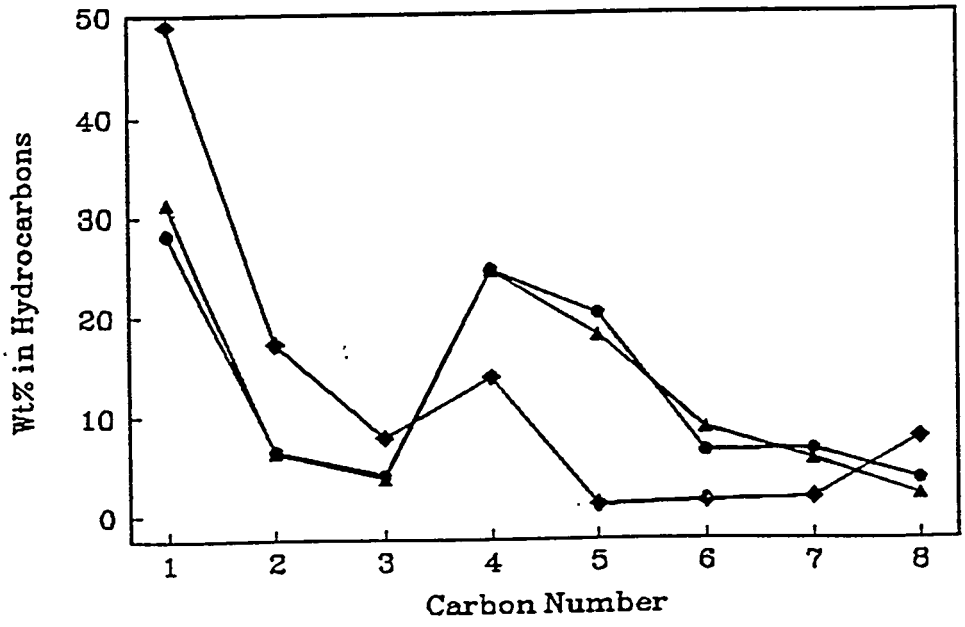

Figure 3.38. Distribution of hydrocarbons at 723 K, 70 atm, 1/1 CO/H_2 ratio, and 80 second space time: ▲-Al_2O_3-ZrO_2 (MSG), ◆-SiO_2-ZrO_2 (MSG), ●-ZrO_2 (MSG).

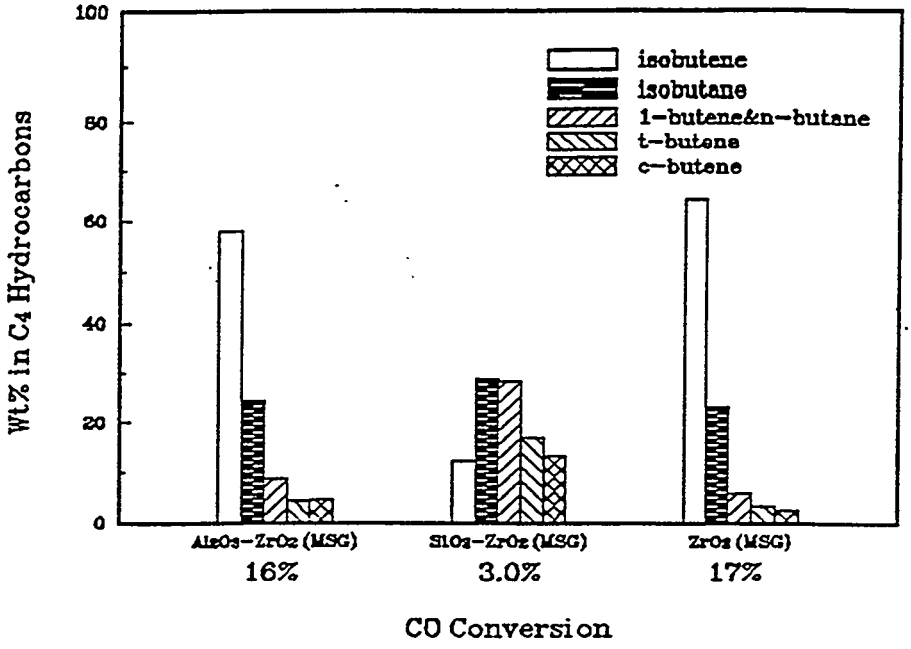

Figure 3.39. Distribution of C_4 hydrocarbons at 723 K, 70 atm, 1/1 CO/H_2 ratio, and 80 second space time.

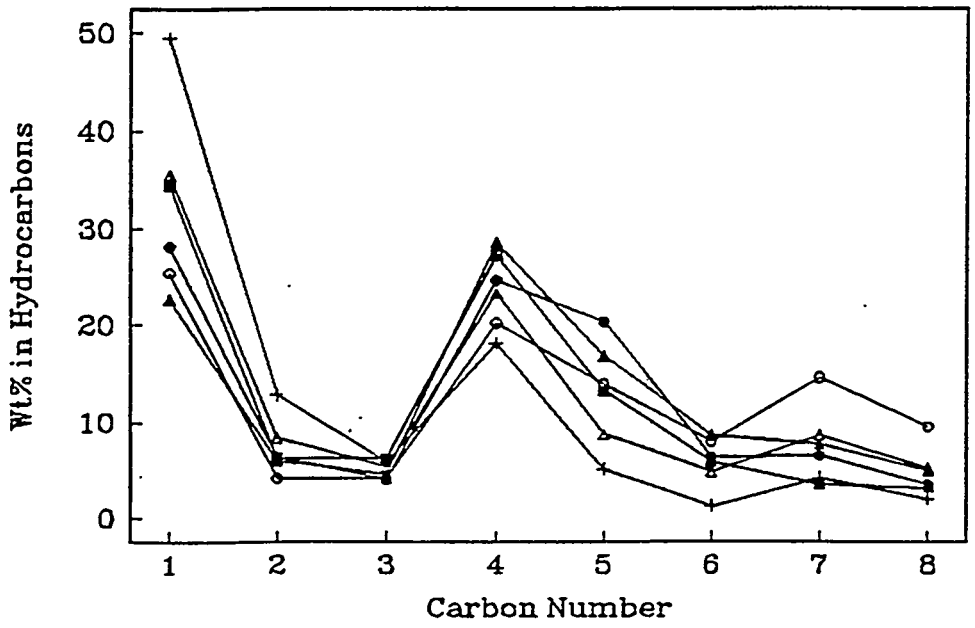

Figure 3.40. Effect of alkali metals on hydrocarbon distribution at 723 K, 70 atm, 1/1 CO/H_2 ratio, and 80 second space time: +-Li-ZrO_2 (MSG), ▵-Na-ZrO_2 (MSG), ▲-K-ZrO_2 (MSG), ○-Rb-ZrO_2 (MSG), ■-Cs-ZrO_2 (MSG), ●-ZrO_2 (MSG).

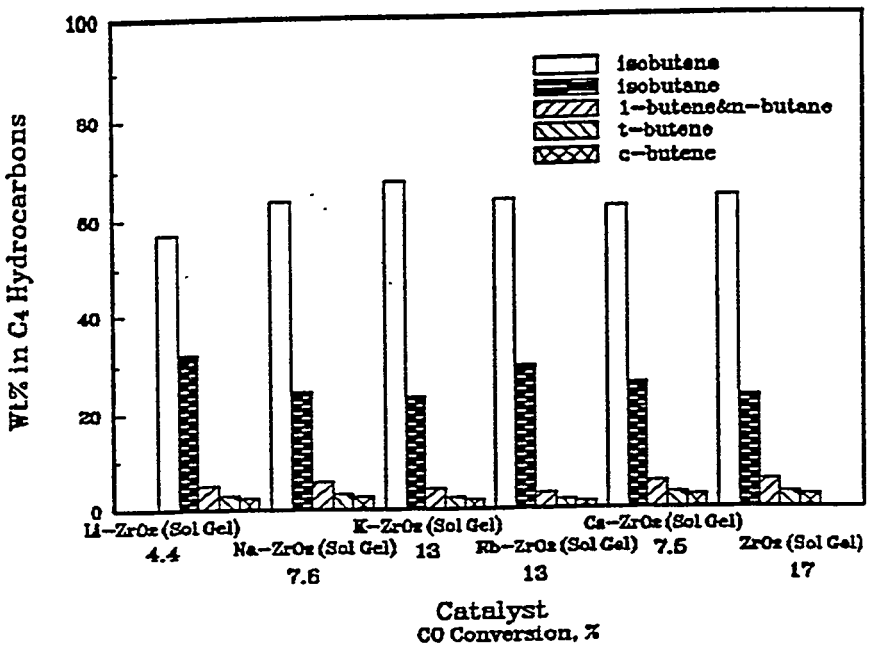

Figure 3.41. C_4 hydrocarbon distribution and CO conversion over alkali promoted catalysts at 723 K, 70 atm, 1/1 CO/H_2 ratio, and 80 second space time.

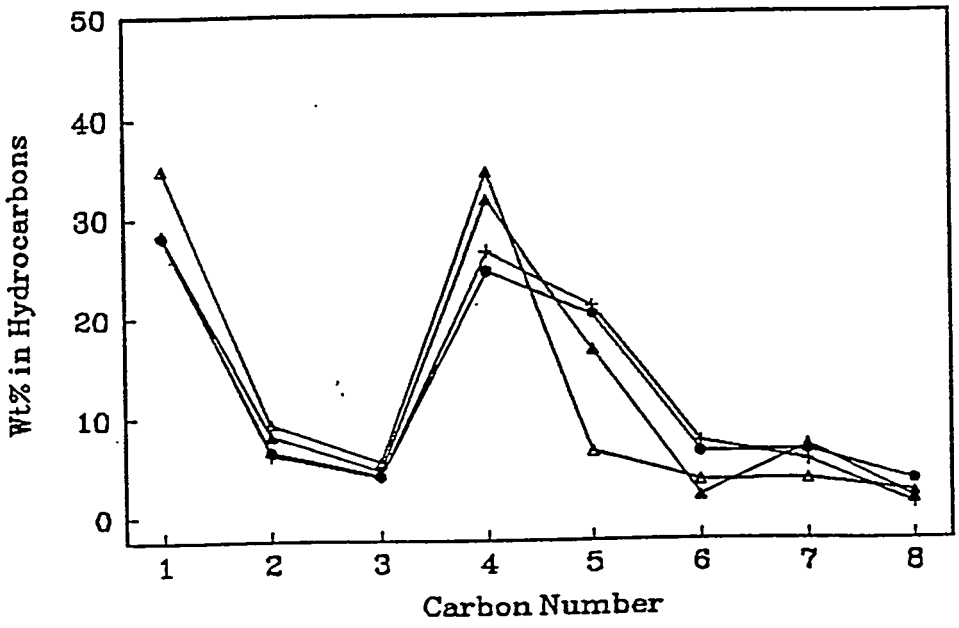

Figure 3.42. Effect of alkaline earth metals on hydrocarbon distribution at 723 K, 70 atm, 1/1 CO/H_2 ratio, and 80 second space time: +-Mg-ZrO_2 (MSG), ▲-Ca-ZrO_2 (MSG), △-Ba-ZrO_2 (MSG), ●-ZrO_2 (MSG).

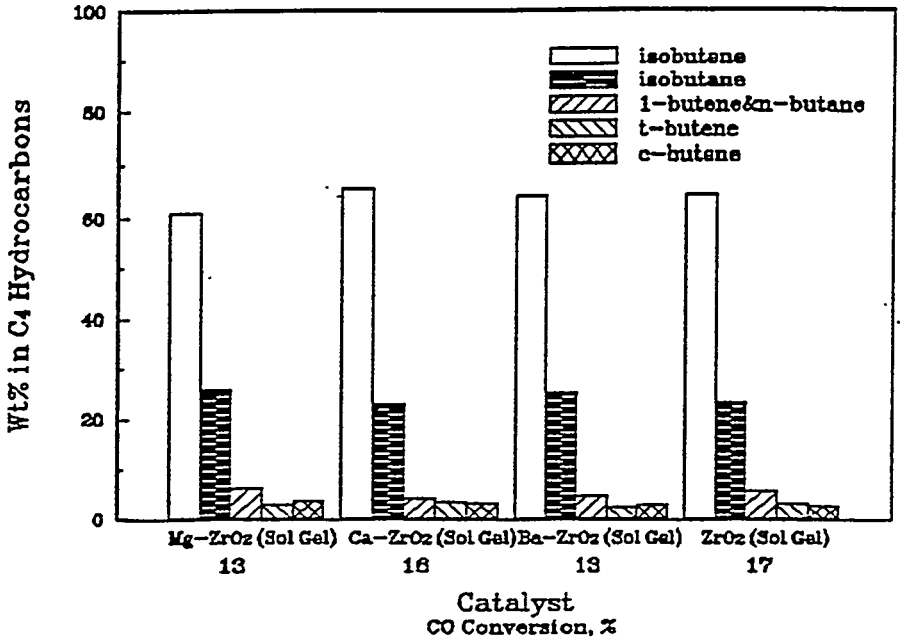

Figure 3.43. C_4 hydrocarbon distribution and CO conversion over alkaline promoted catalysts at 723 K, 70 atm, 1/1 CO/H_2 ratio, and 80 second space time.

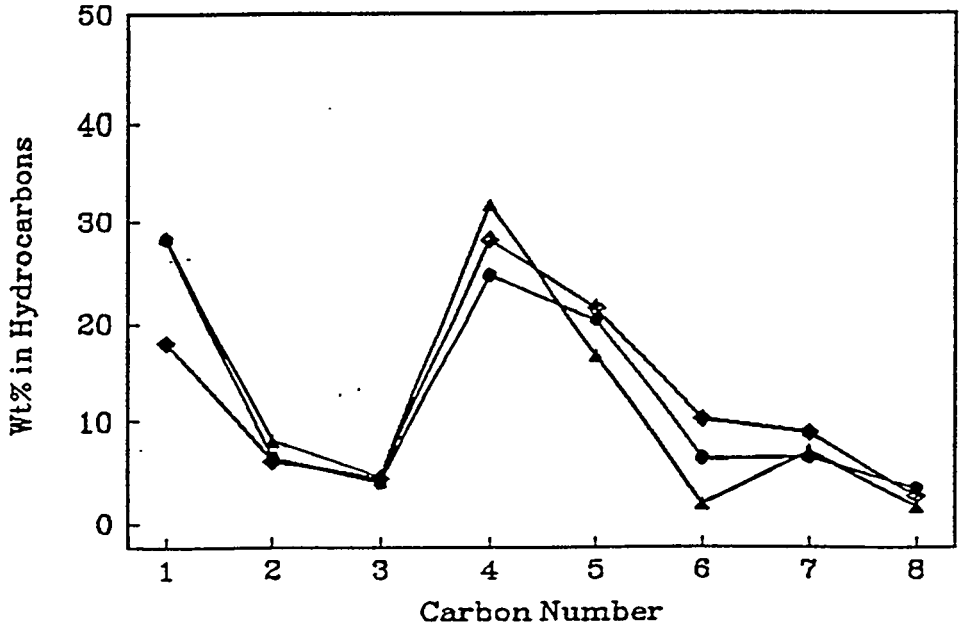

Figure 3.44. Effect of calcium loading on hydrocarbon distribution at 723 K, 70 atm, 1/1 CO/H_2 ratio, and 80 second space time: ♦-Ca(2%)-ZrO_2 (MSG), ▲-Ca-ZrO_2 (MSG), ●-ZrO_2 (MSG).

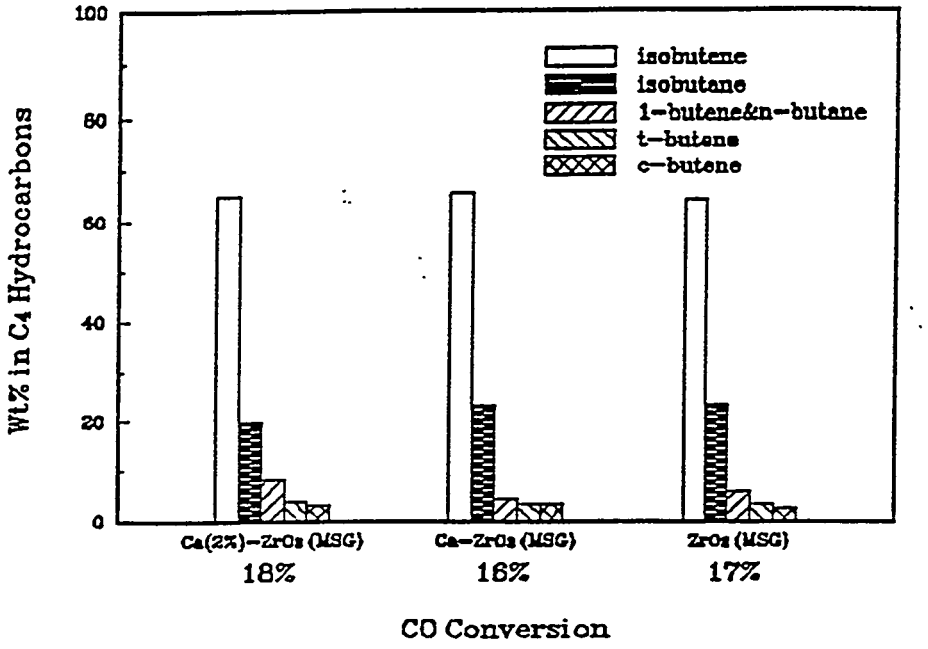

Figure 3.45. Effect of calcium loading on C_4 hydrocarbon distribution at 723 K, 70 atm, 1/1 CO/H_2 ratio, and 80 second space time.

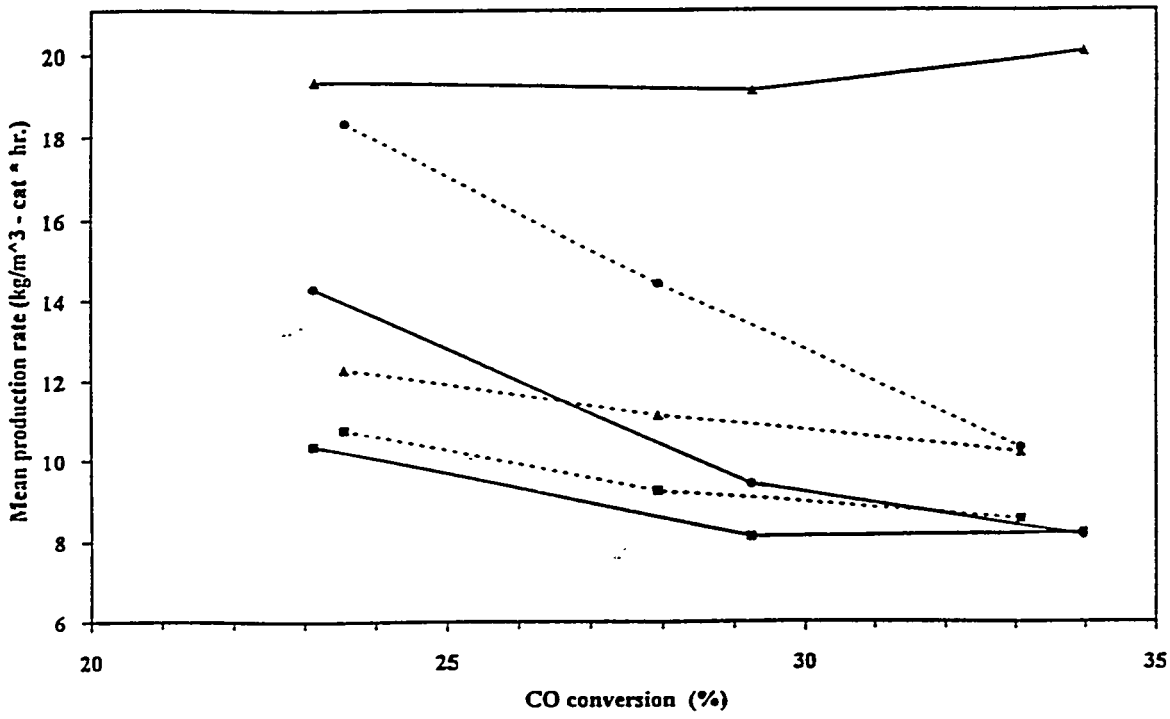

Figure 3.46. Comparison of mean production rates for non-H_2S (solid line) and H_2S (dashed line) runs for methane (▲), total C_4 (■), and C_5+ (●) at 673 K, 50 atm, and 1/1 CO/H_2 [or $CO/(H_2+H_2S)$] ratio.

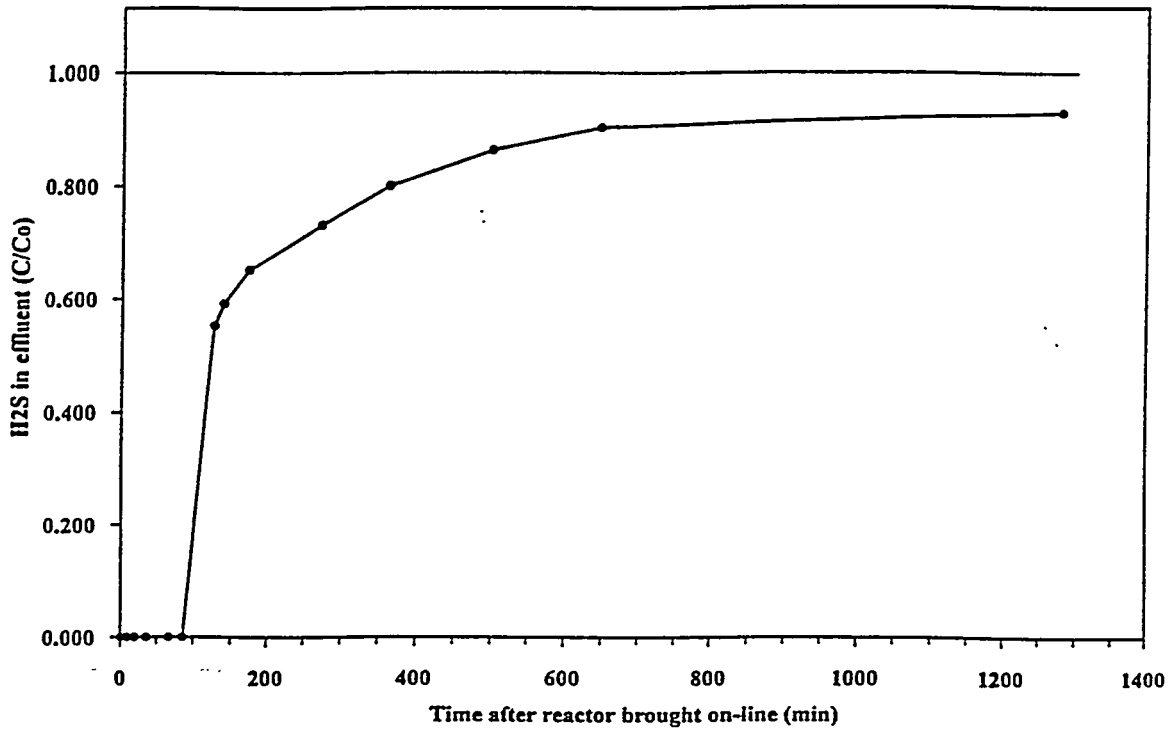

Figure 3.47. Breakthrough curve for H_2S over 7% Ce-ZrO_2 at 673 K, 25 atm, and 90 second space time.

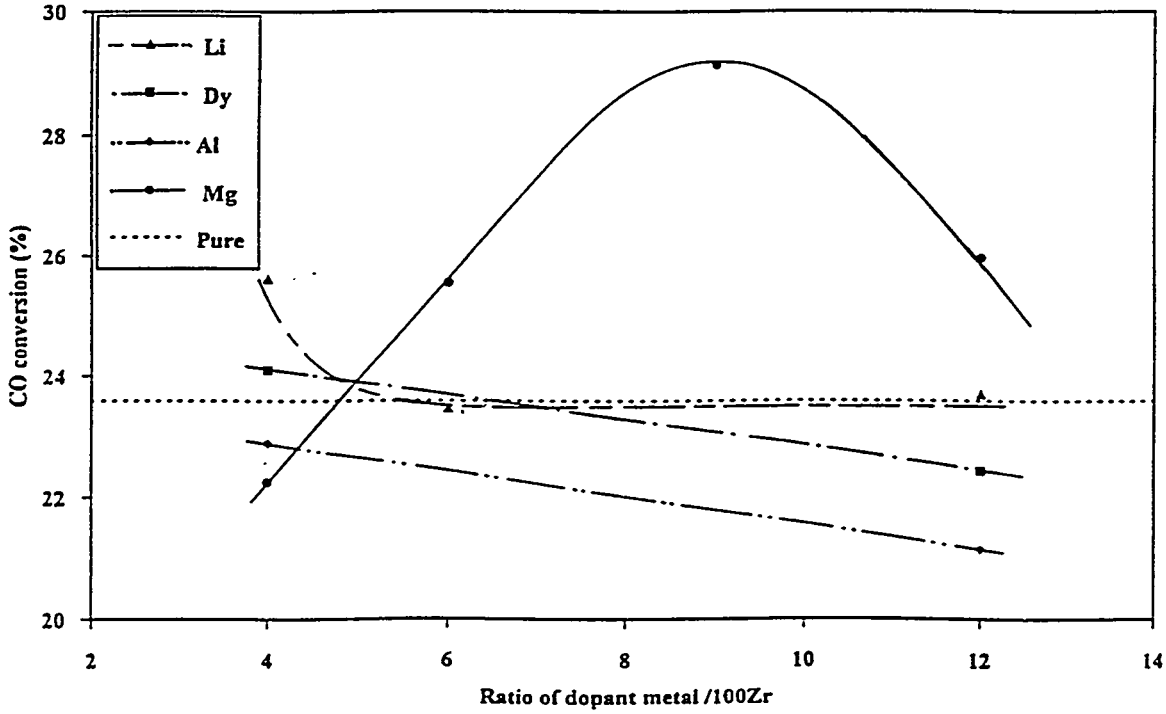

Figure 3.48. Changes in CO conversion with dopant level at 673 K, 50 atm, 1/1 CO/H_2 ratio, and 90 second space time.

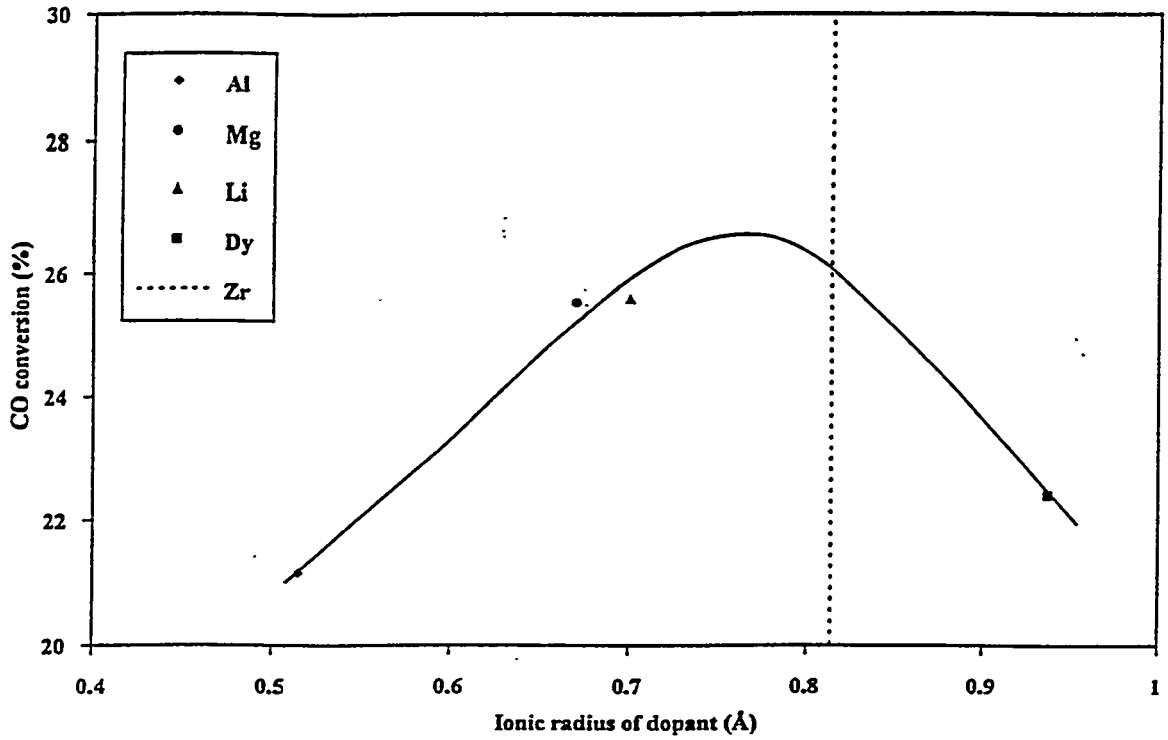

Figure 3.49. Changes in CO conversion with ionic radius of the dopant cation at an oxygen vacancy to zirconium ratio of 0.06 at 673 K, 50 atm, 1/1 CO/H_2 ratio, and 90 second space time.

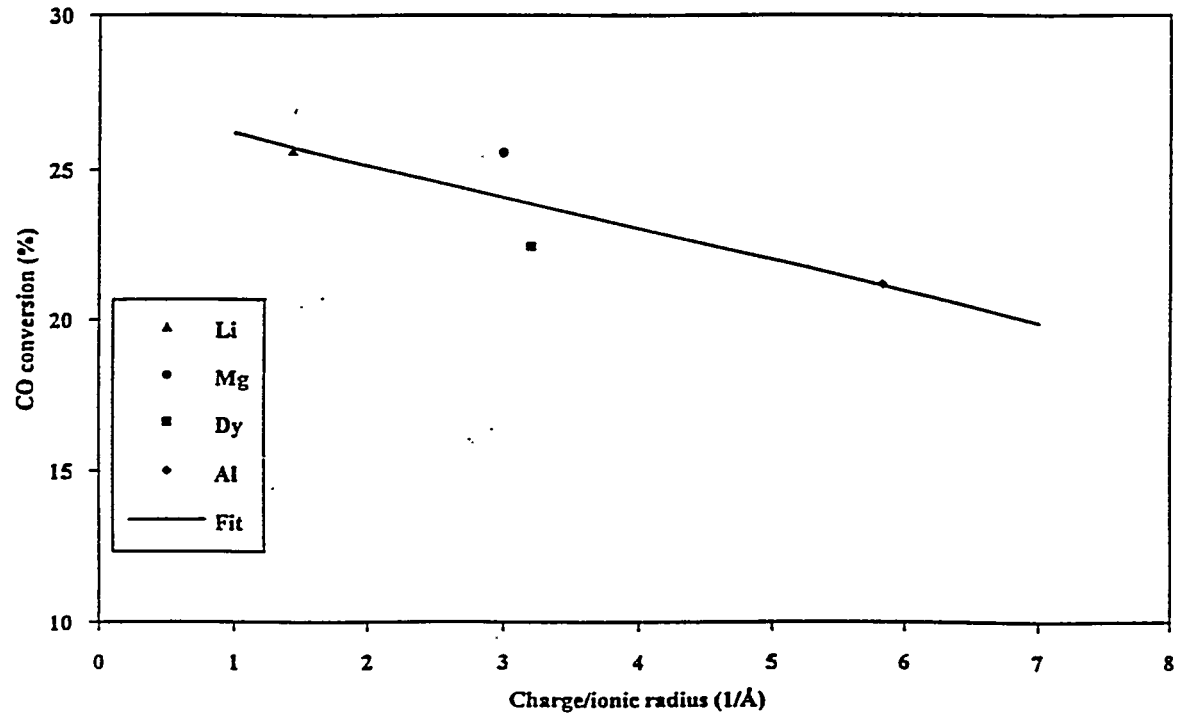

Figure 3.50. Changes in CO conversion with dopant charge to ionic radius ratio at an oxygen vacancy to zirconium ratio of 0.06 at 673 K, 50 atm, 1/1 CO/H_2 ratio, and 90 second space time.

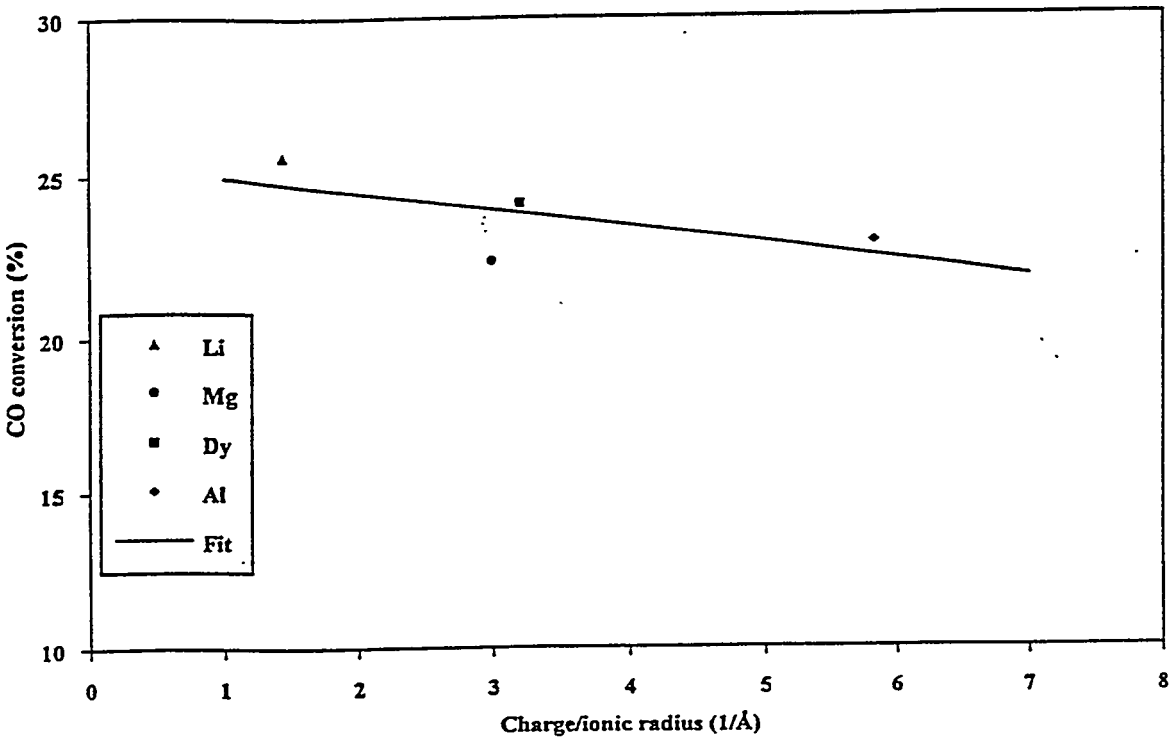

Figure 3.51. Changes in CO conversion with dopant charge to ionic radius ratio at a dopant metal to zirconium ratio of 0.04 at 673 K, 50 atm, 1/1 CO/H_2 ratio, and 90 second space time.

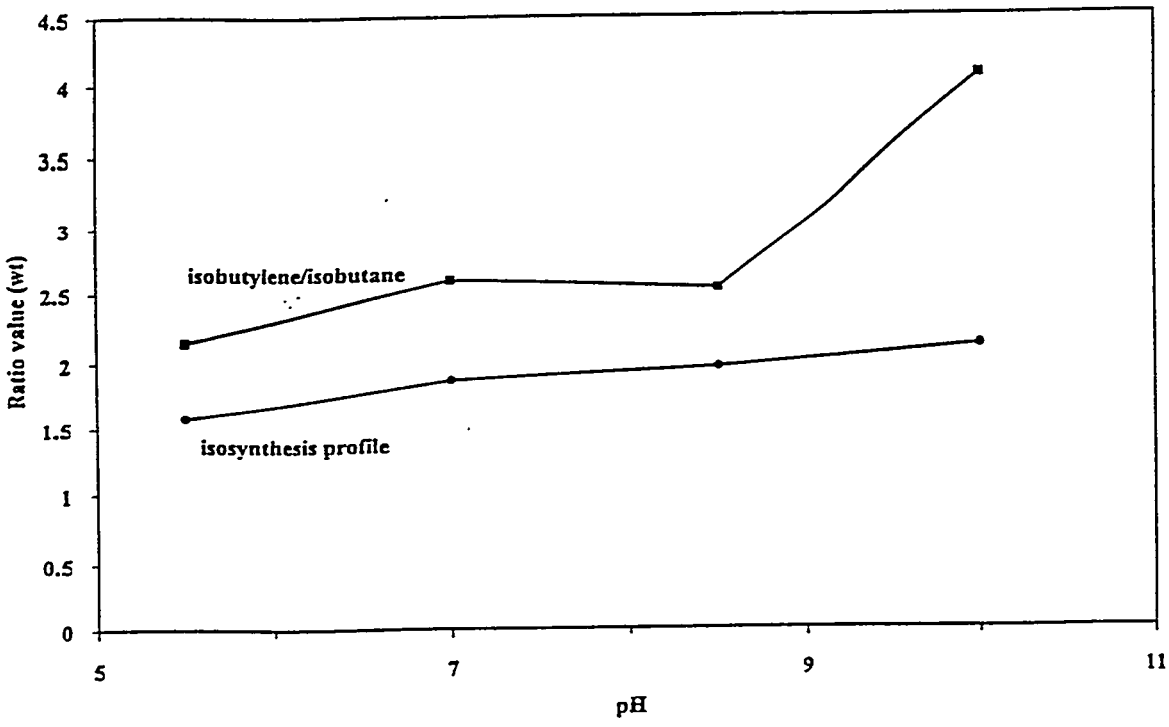

Figure 3.52. Changes in isobutylene/isobutane ratio and isosynthesis profile with *p*H at 673 K, 50 atm, 1/1 CO/H_2 ratio, and 90 second space time.

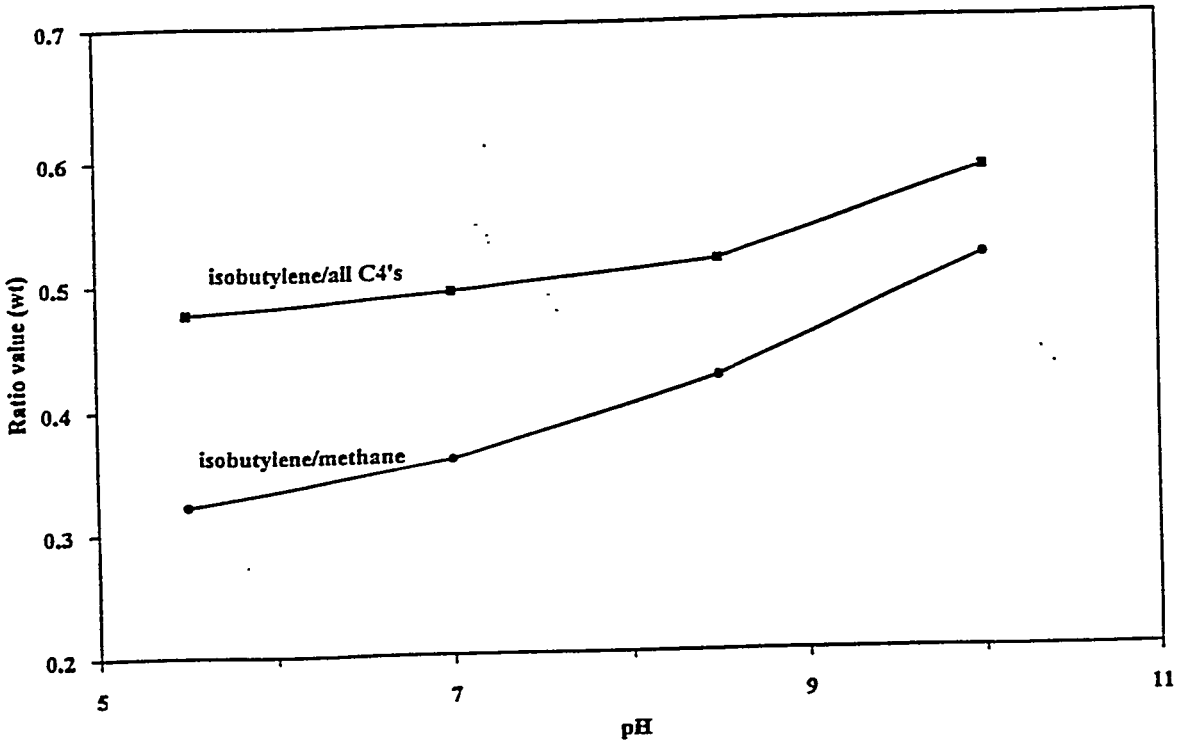

Figure 3.53. Changes in isobutylene fraction among C_4's and isobutylene/methane ratio with *p*H at 673 K, 50 atm, 1/1 CO/H_2 ratio, and 90 second space time.

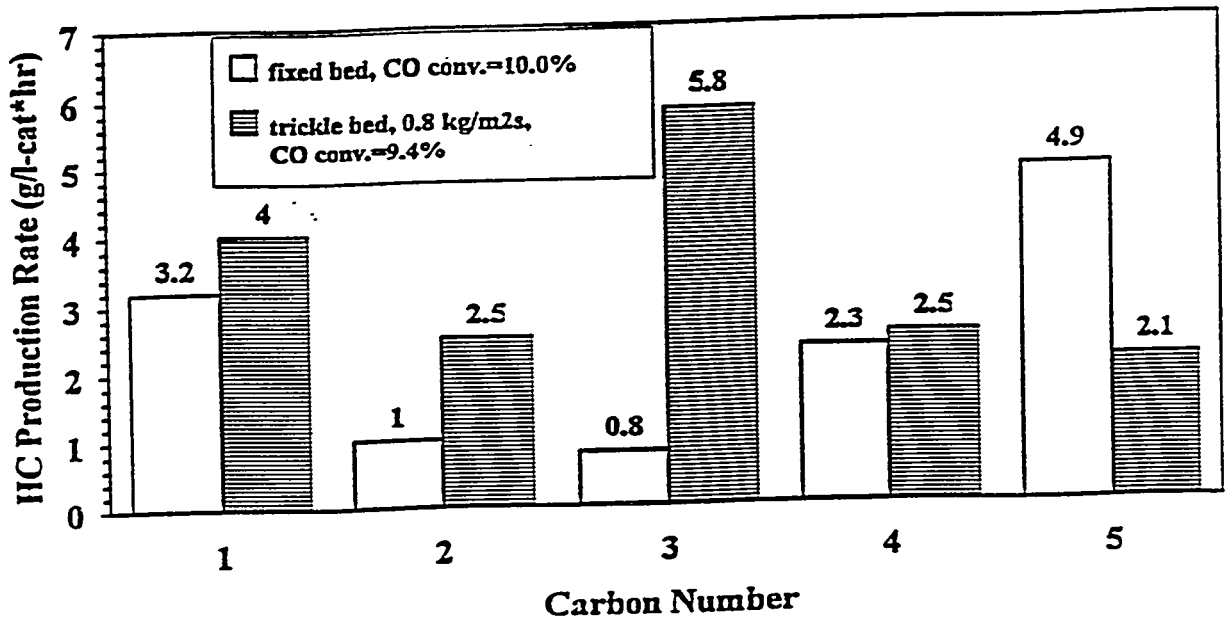

Figure 3.54. Comparison of the hydrocarbon distribution for fixed and trickle bed reactors at 669 K, 51 atm, 1/1 CO/H_2 ratio and 89 second space time.

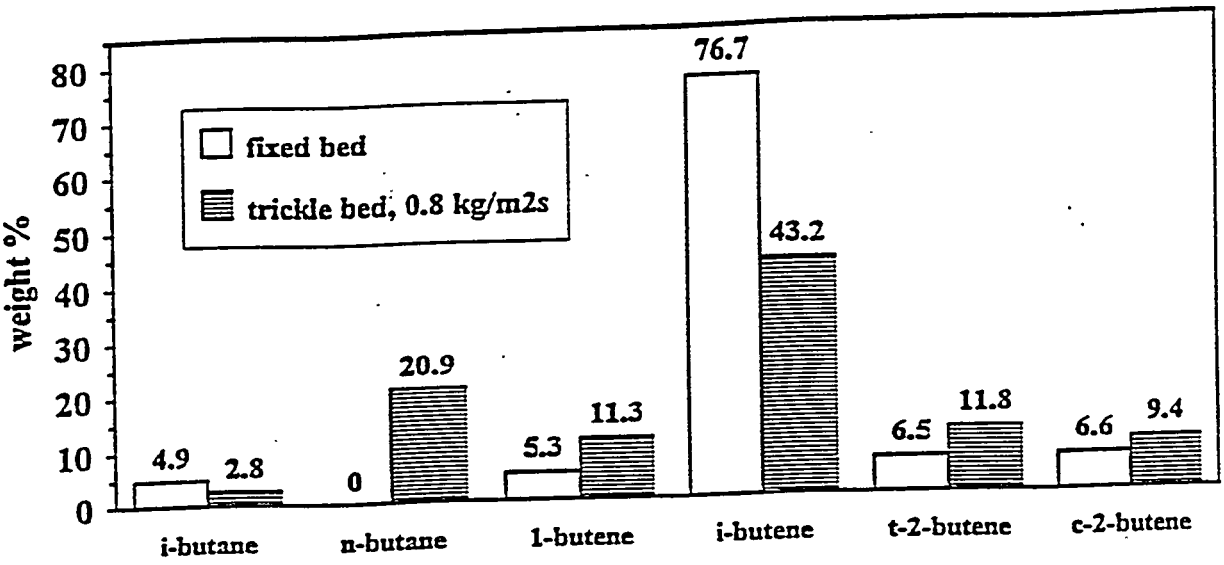

Figure 3.55. Comparison of C_4 distribution for fixed and trickle bed reactors at 669 K, 51 atm, 1/1 CO/H_2 ratio, and 89 second space time.

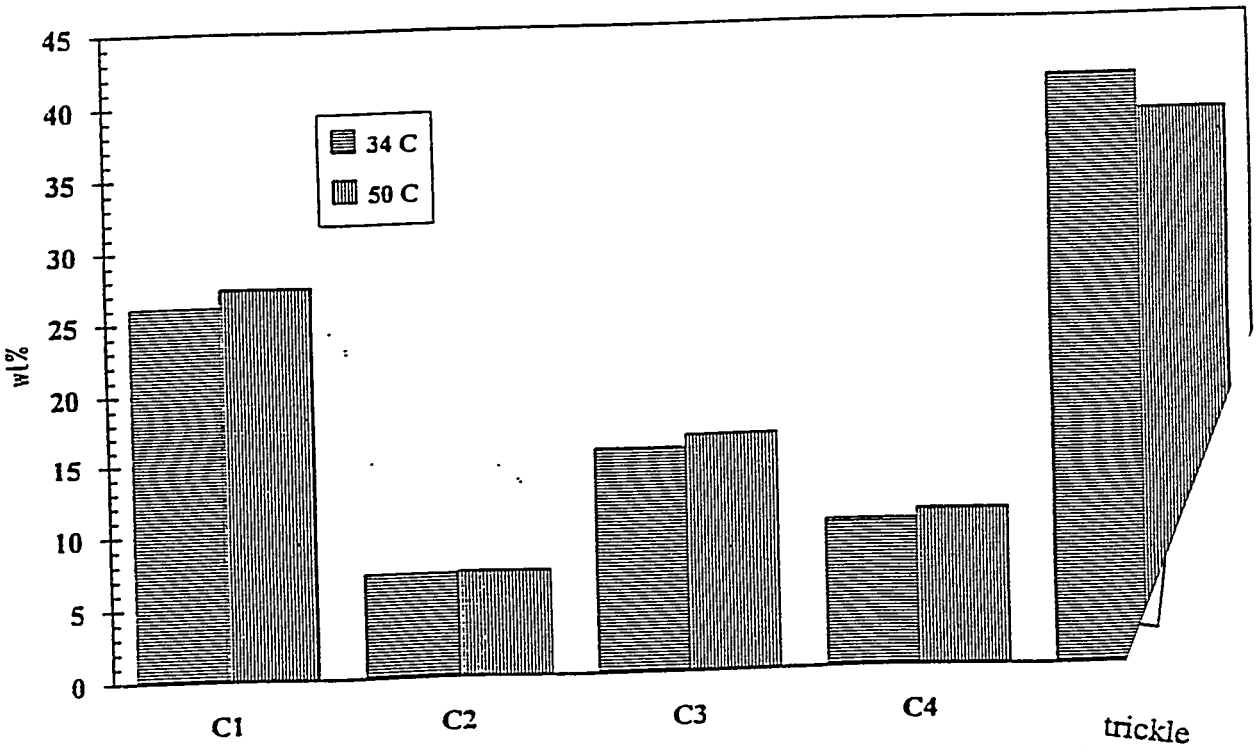

Figure 3.56. Effect of gas oil separator temperature on hydrocarbon distributi[illegible]econd bed reactor at 10% CO conversion, 669 K, 51 atm, 1/1 CO/H_2 space time.

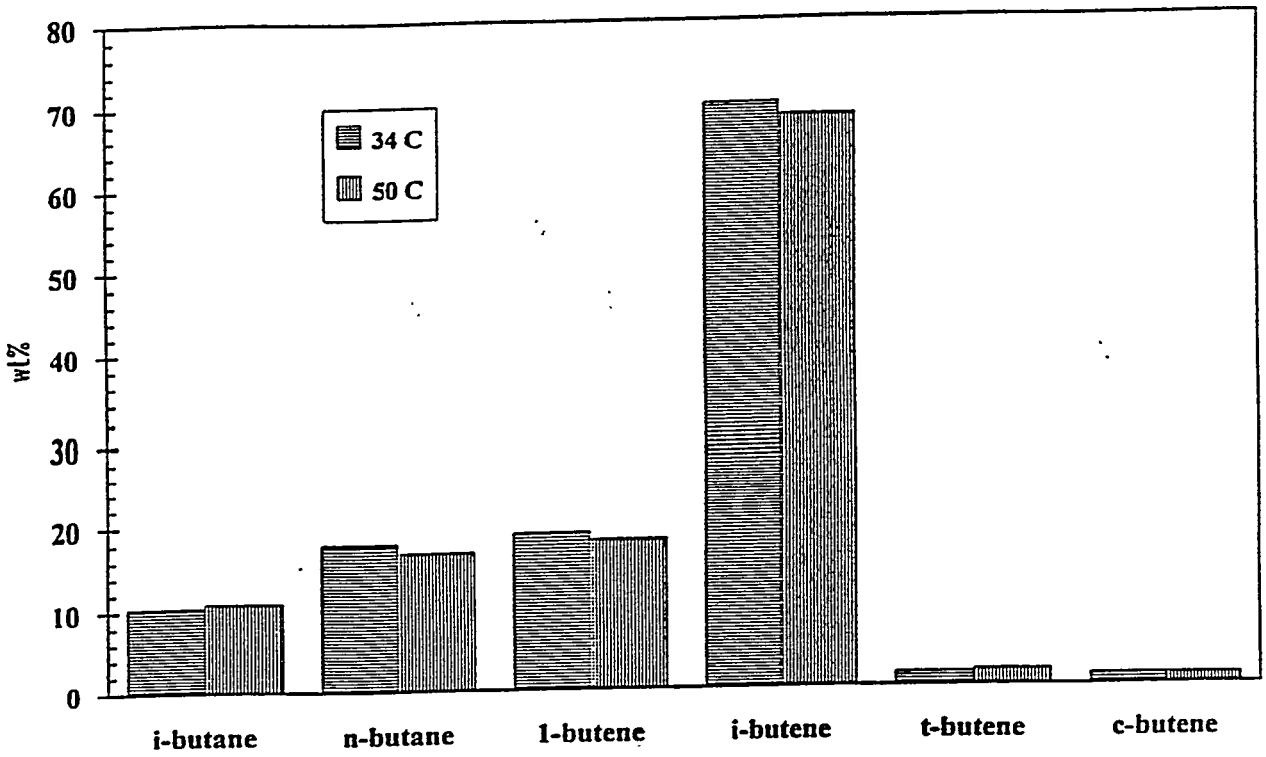

Figure 3.57. Effect of gas oil separator temperature on C_4 distribution in the trickle bed reactor at 10% CO conversion, 669 K, 51 atm, 1/1 CO/H_2 ratio, and 89 second space time.

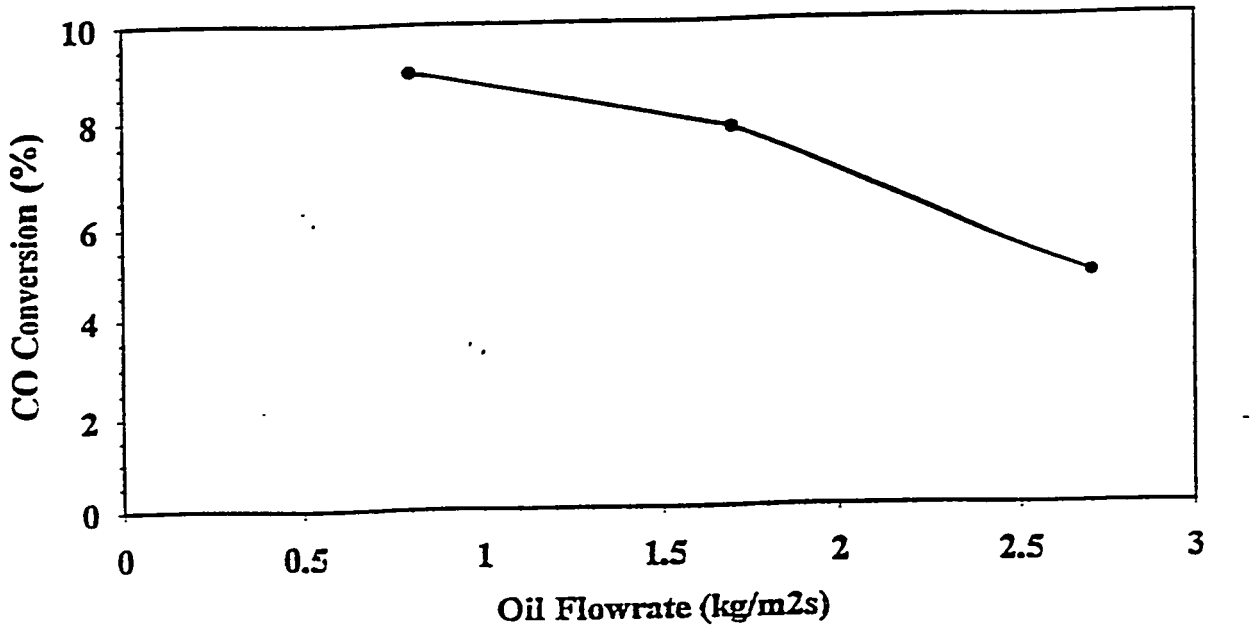

Figure 3.58. Variation of CO conversion with oil flow rate in the trickle bed reactor at 669 K, 51 atm, 1/1 CO/H_2 ratio, and 668 (1/hr) space velocity.

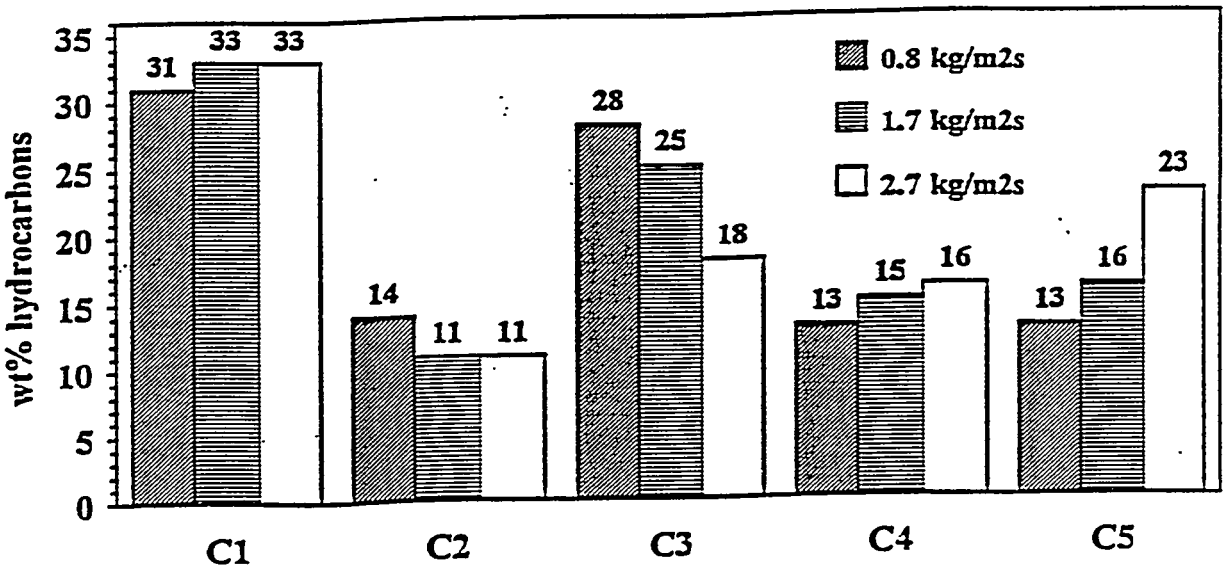

Figure 3.59. Change in hydrocarbon distribution with oil flow rate in the trickle bed reactor at 669 K, 51 atm, 1/1 CO/H_2 ratio, and 668 (1/hr) space velocity.

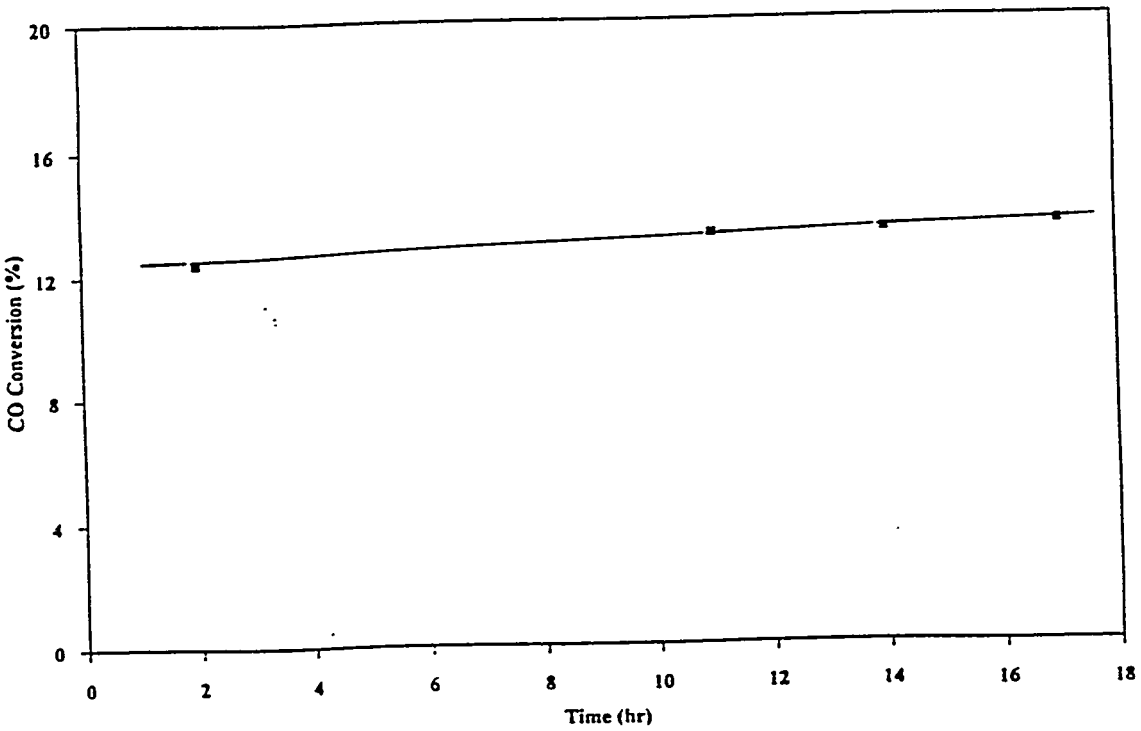

Figure 3.60. Changes in CO conversion level with time on stream in the slurry reactor over ZrO_2 (ppt.).

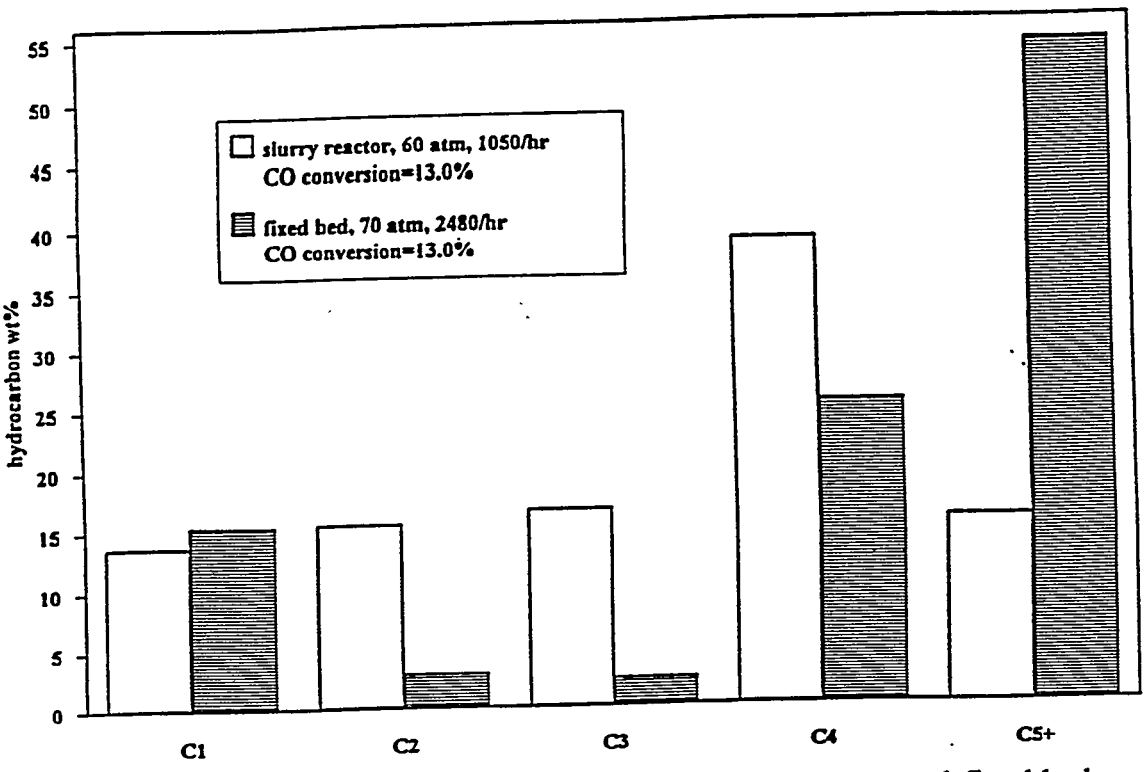

Figure 3.61. Comparison of hydrocarbon distribution between slurry and fixed bed reactors over ZrO_2 (ppt.).

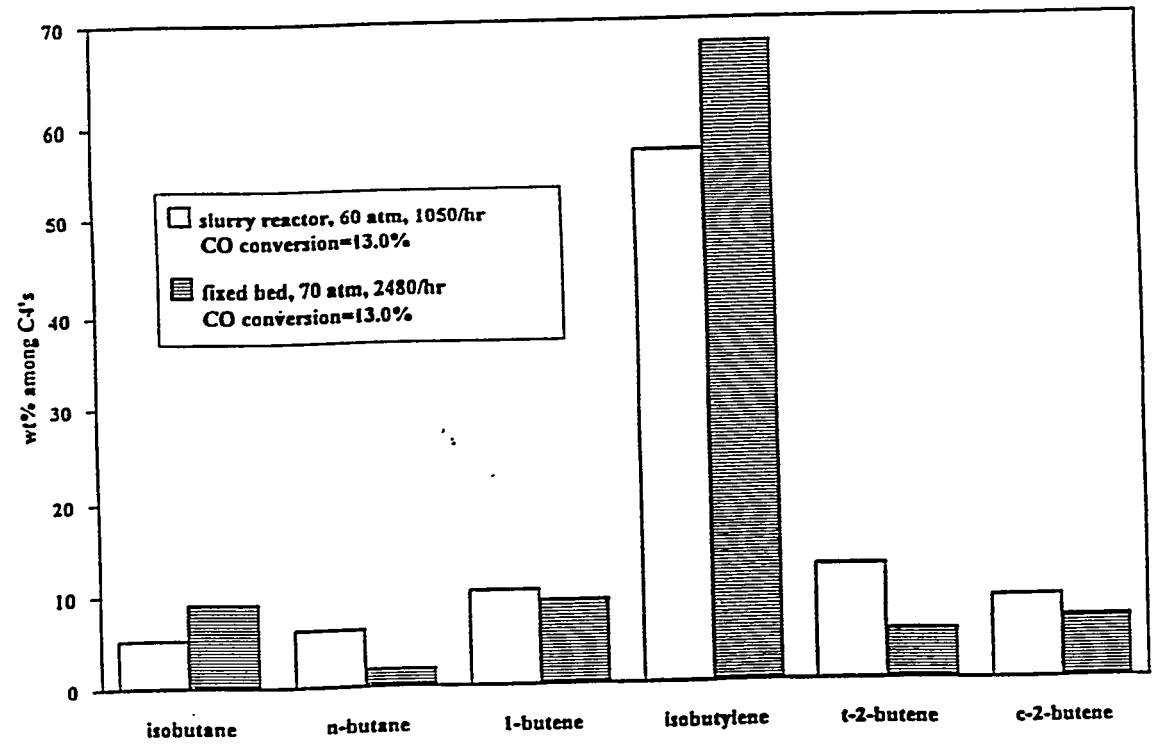

Figure 3.62. Comparison of C_4 distribution between slurry and fixed bed reactors over ZrO_2 (ppt.).

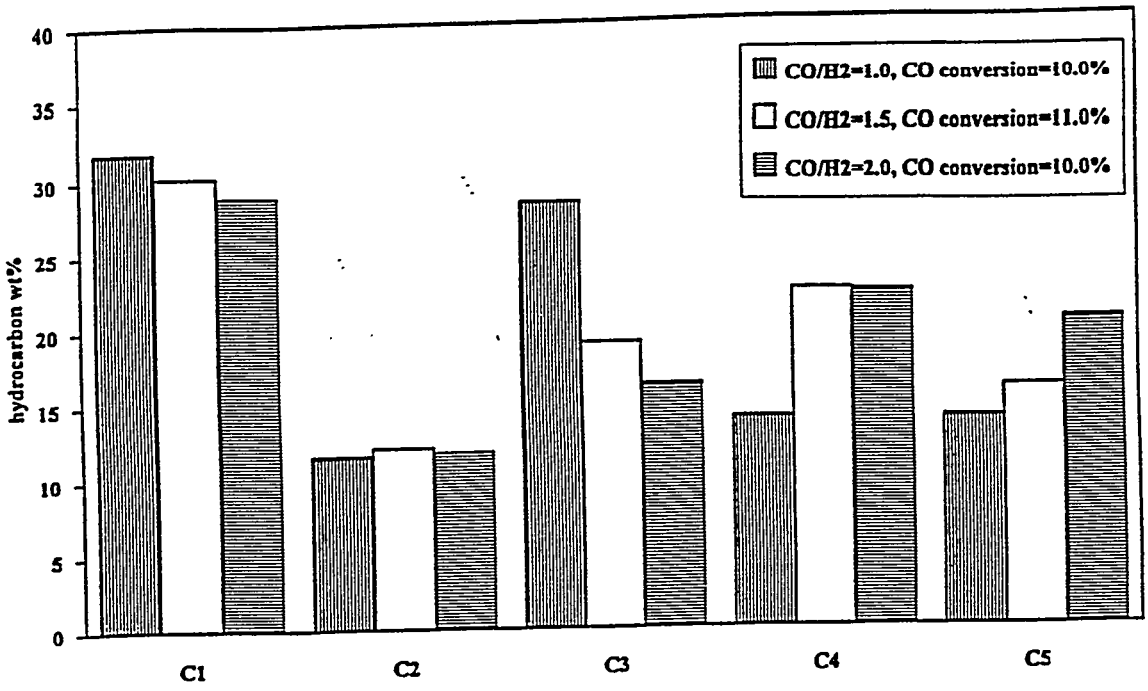

Figure 3.63. Changes in hydrocarbon distribution with CO/H_2 ratio in the slurry reactor over commercial ZrO_2.

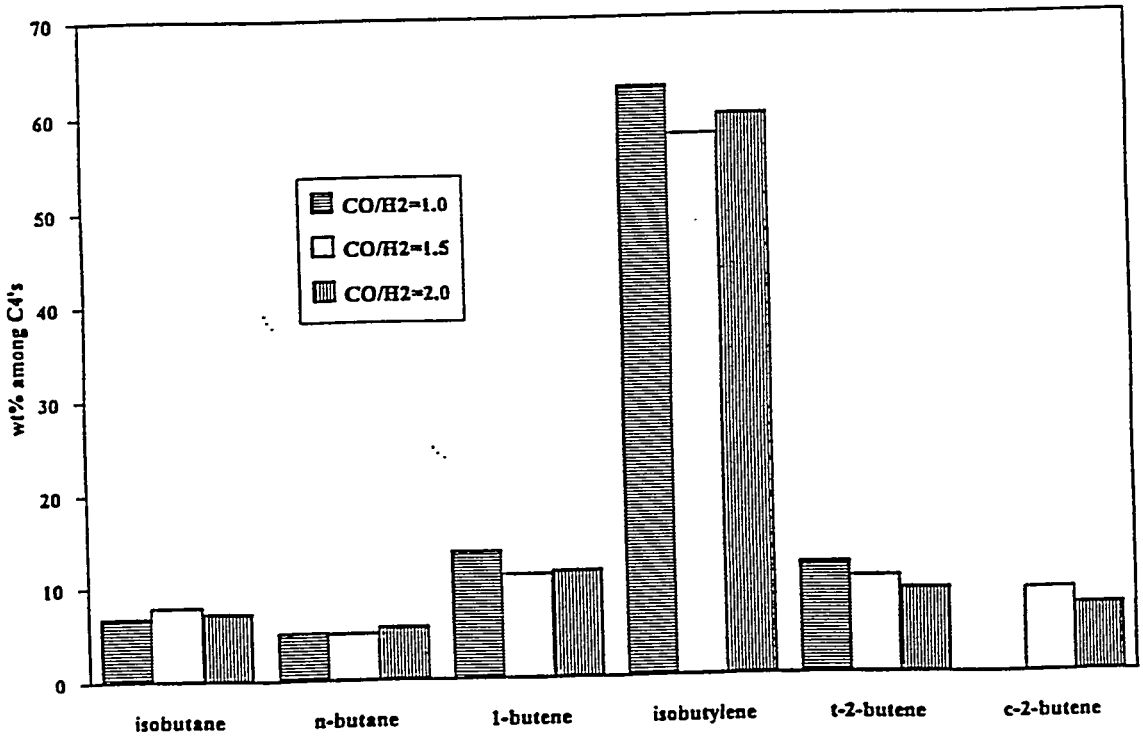

Figure 3.64. Changes in C_4 distribution with CO/H_2 ratio in the slurry reactor over commercial ZrO_2.

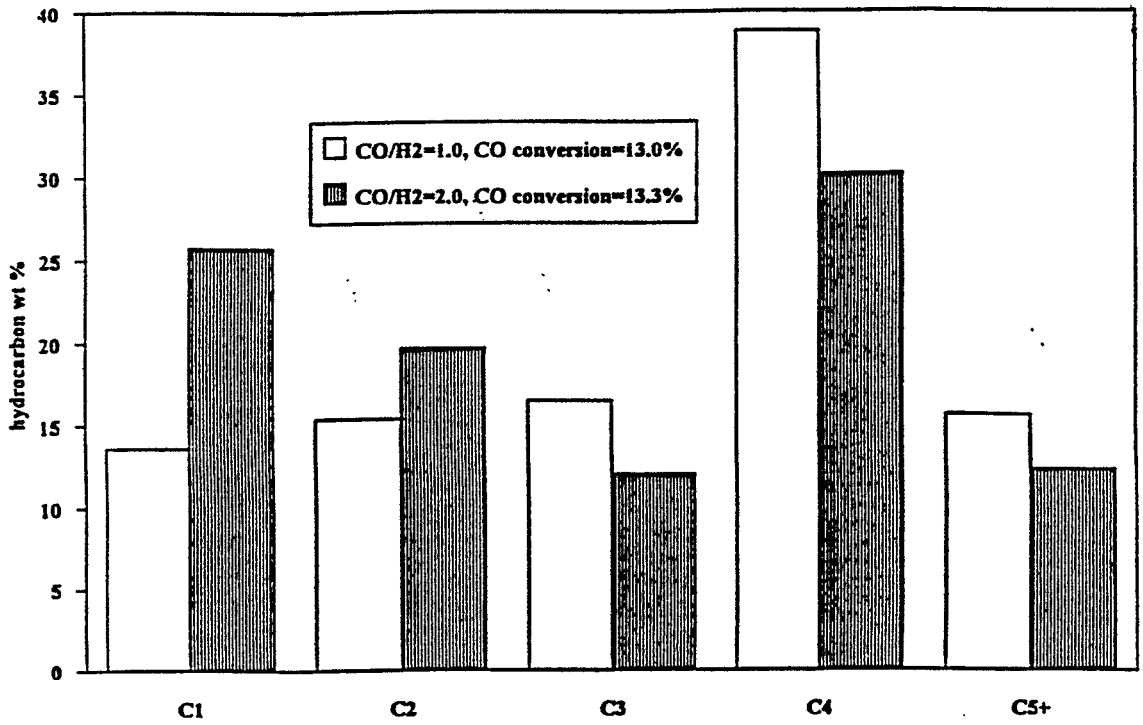

Figure 3.65. Changes in Hydrocarbon distribution with CO/H_2 ratio in the slurry reactor over ZrO_2 (ppt.).

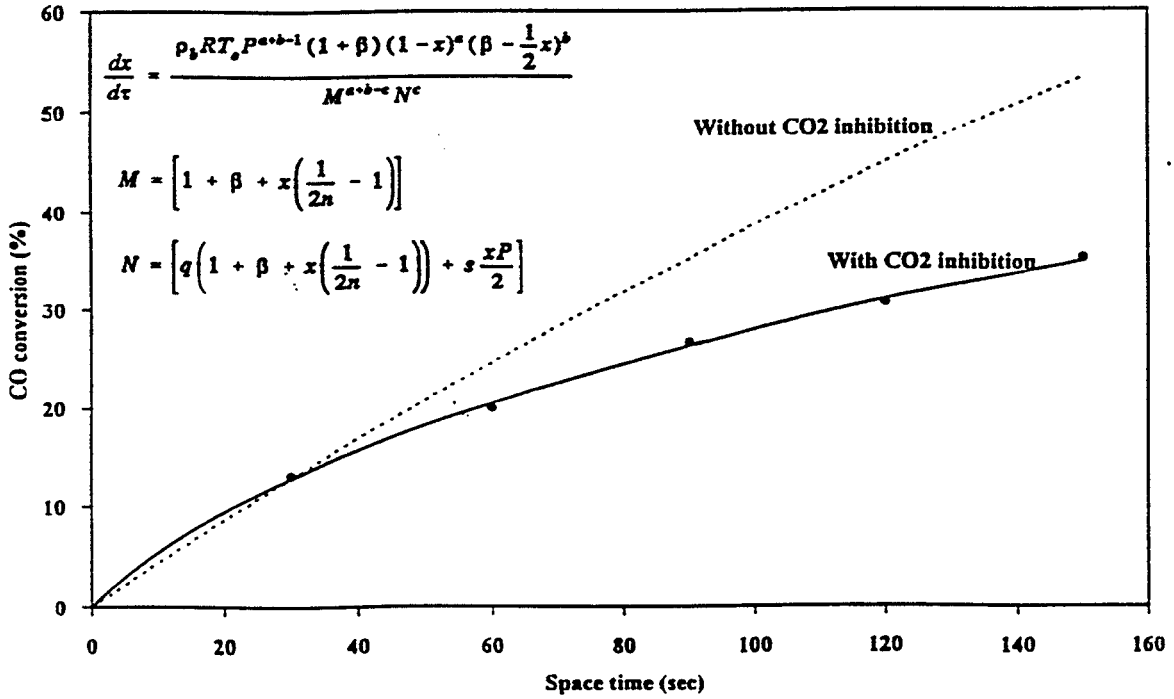

Figure 3.66. Predicted conversion over 7% Ce-ZrO_2 at 673 K, 50 atm, and 1/1 CO/H_2 ratio, with and without CO_2 inhibition.

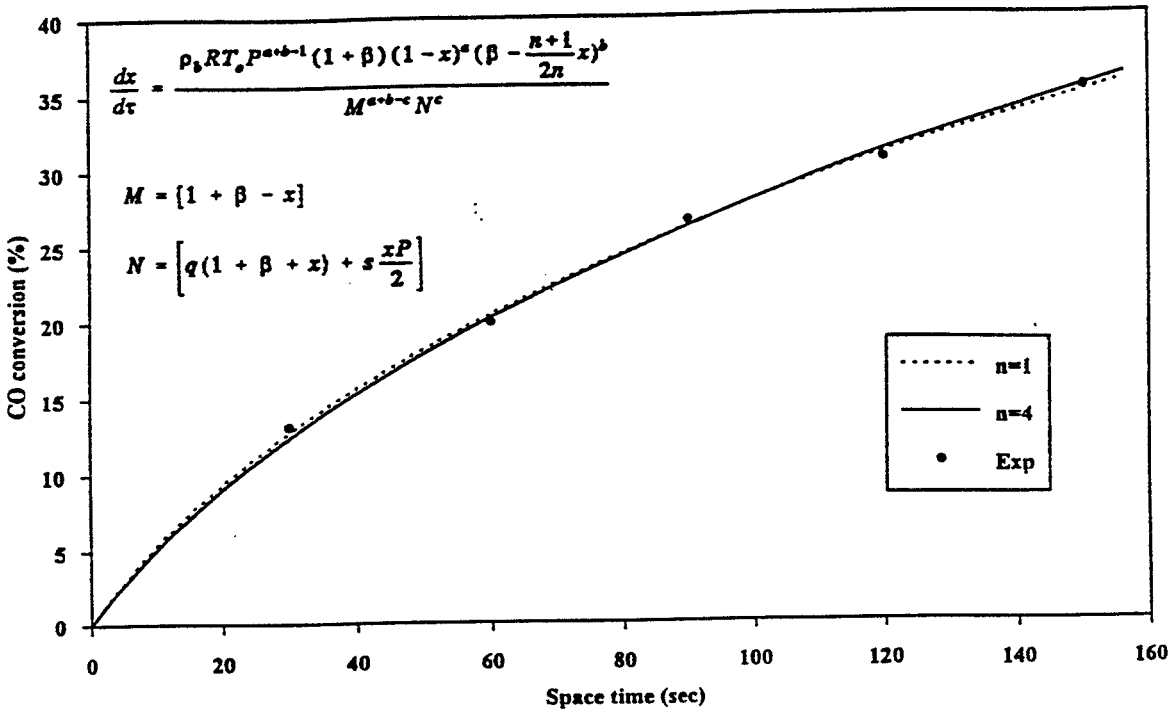

Figure 3.67. Changes in predicted conversion over 7% Ce-ZrO_2 at 673 K, 50 atm, and 1/1 CO/H_2 ratio with *n*.

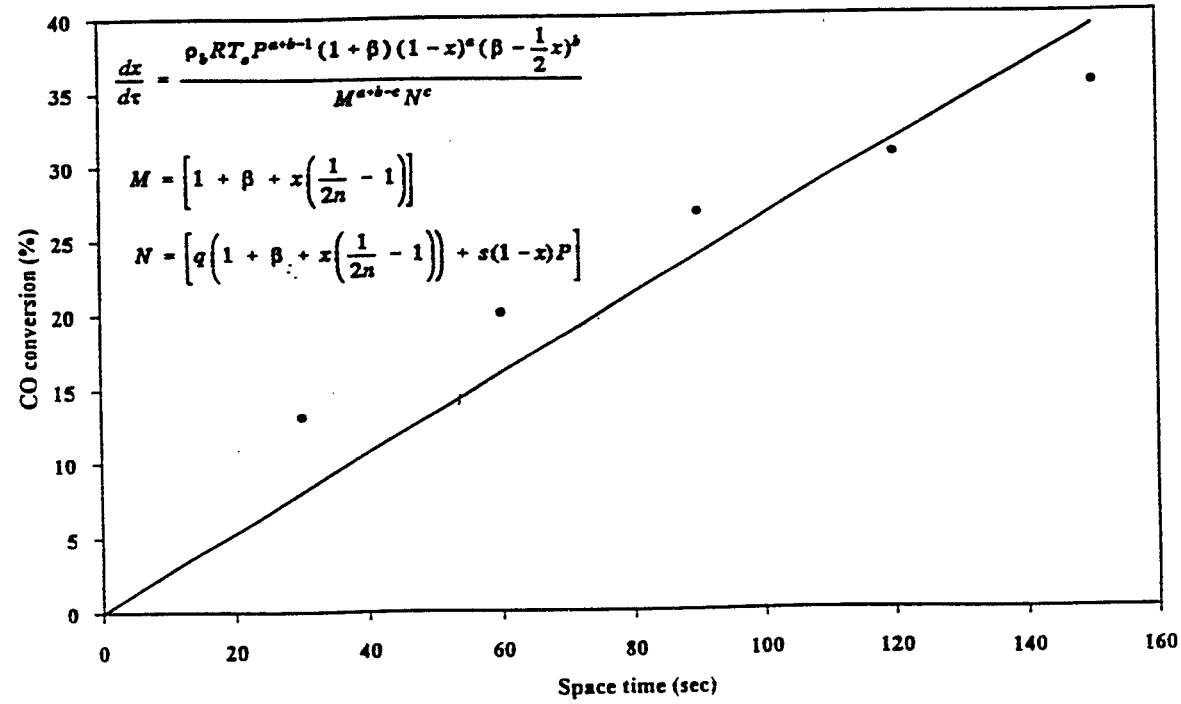

Figure 3.68. Predicted conversion over 7% Ce-ZrO_2 at 673 K, 50 atm, and 1/1 CO/H_2 ratio with CO inhibition.

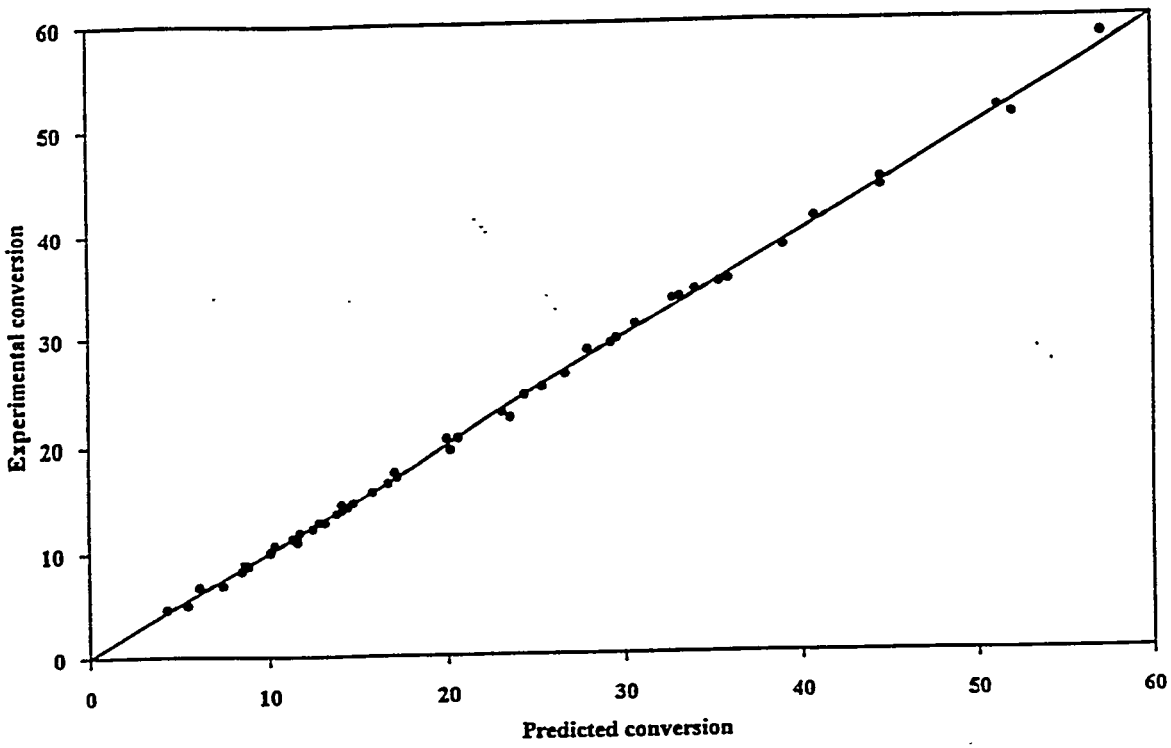

Figure 3.69. Comparison of experimental and predicted carbon monoxide conversion for all catalysts.

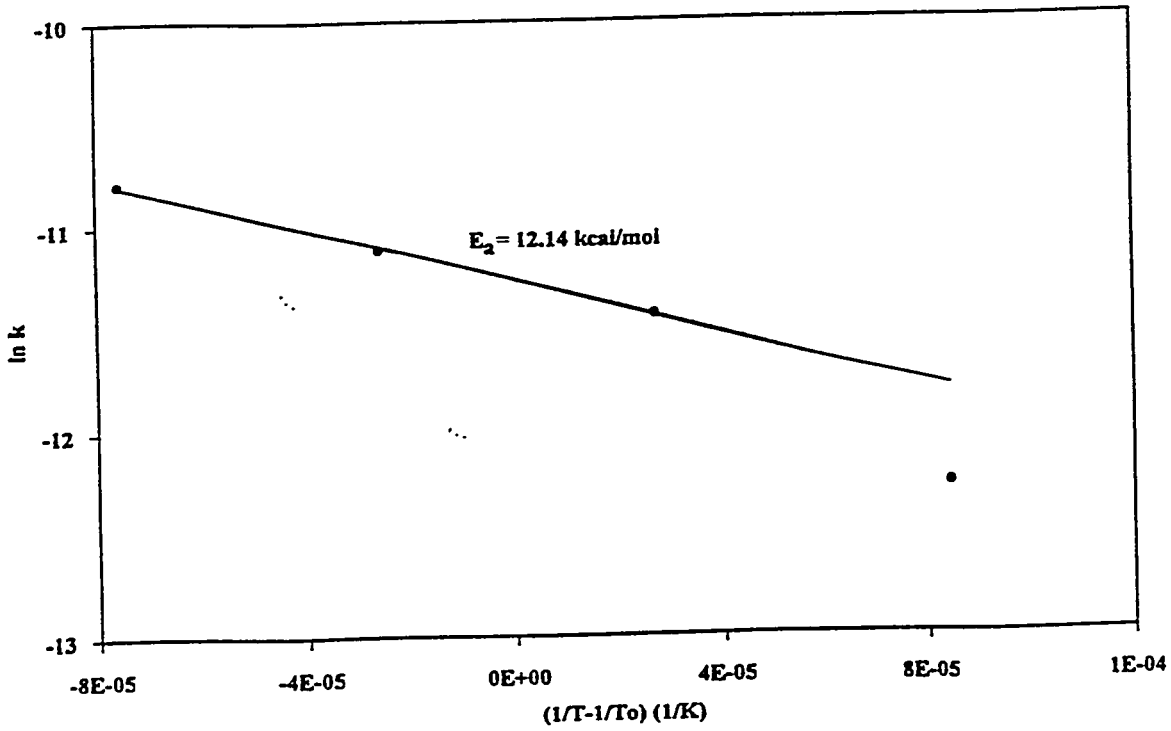

Figure 3.70. Determination of activation energy over 7% Ce-ZrO_2 (ppt.) with aluminum CO cylinder at 50 atm and 1/1 CO/(H_2+H_2S) ratio.

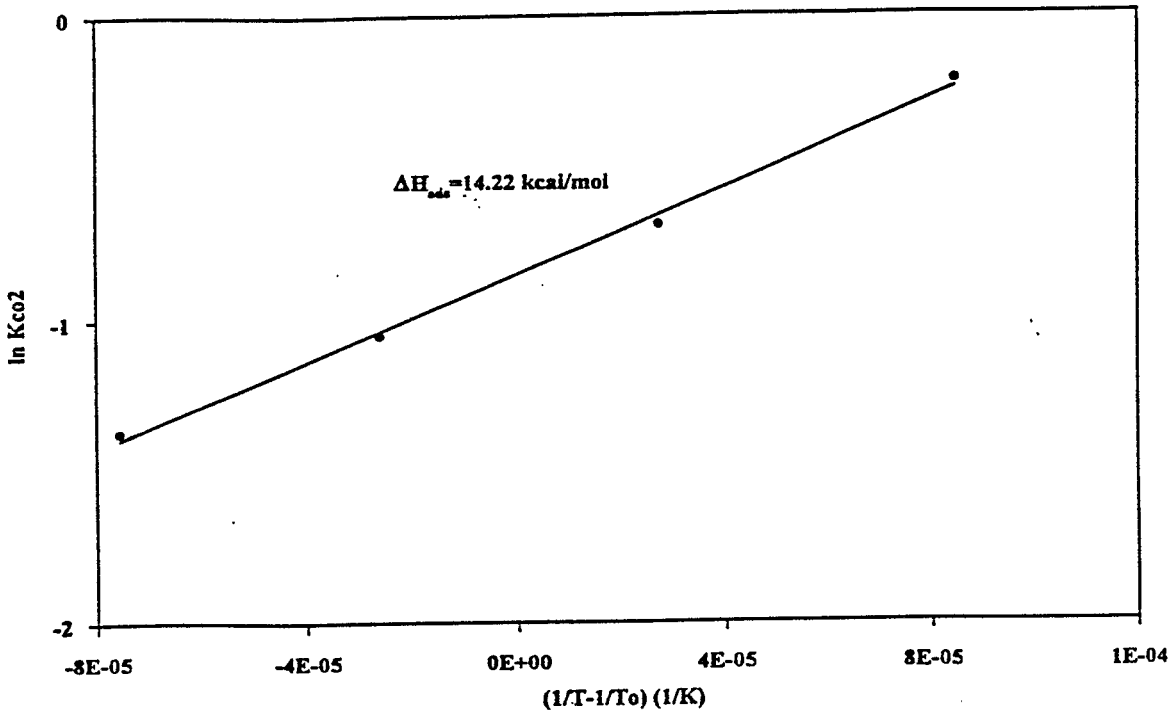

Figure 3.71. Determination of the heat of adsorption for CO_2 over 7% Ce-ZrO_2 (ppt.) with aluminum CO cylinder at 50 atm and 1/1 CO/(H_2+H_2S) ratio.

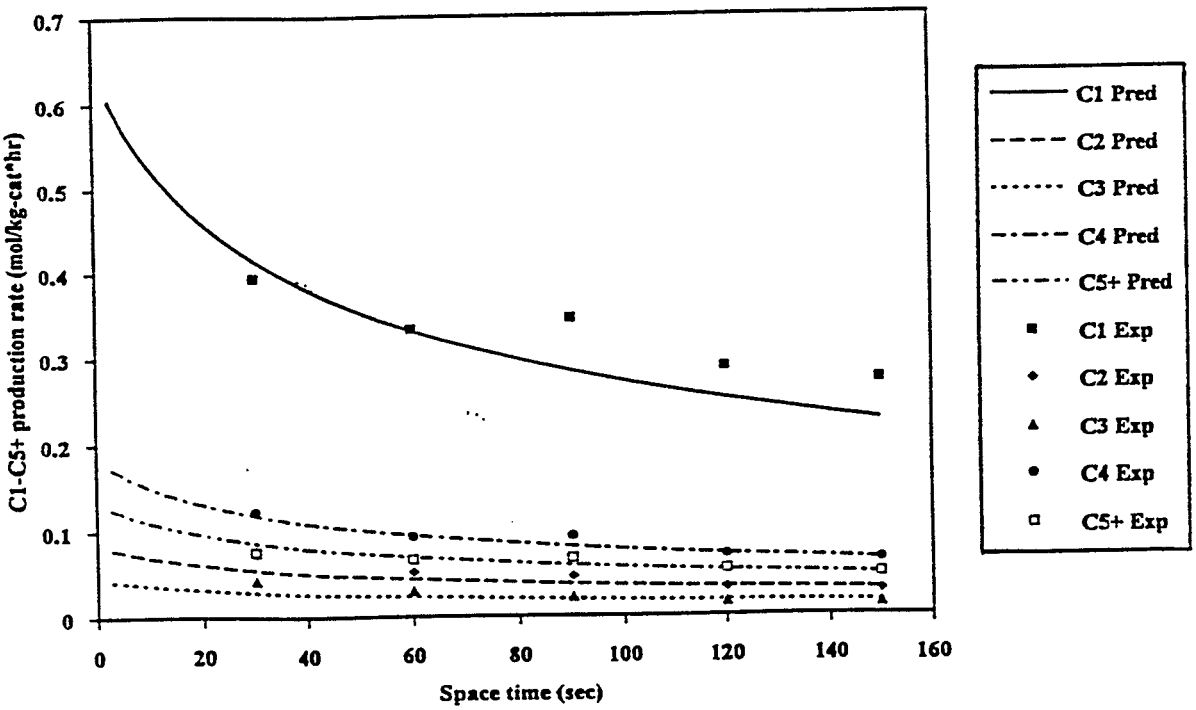

Figure 3.72. Comparison of experimental and predicted C_1-C_5+ production rates over 7% Ce-ZrO_2 at 673 K, 50 atm, and 1/1 CO/H_2 ratio.

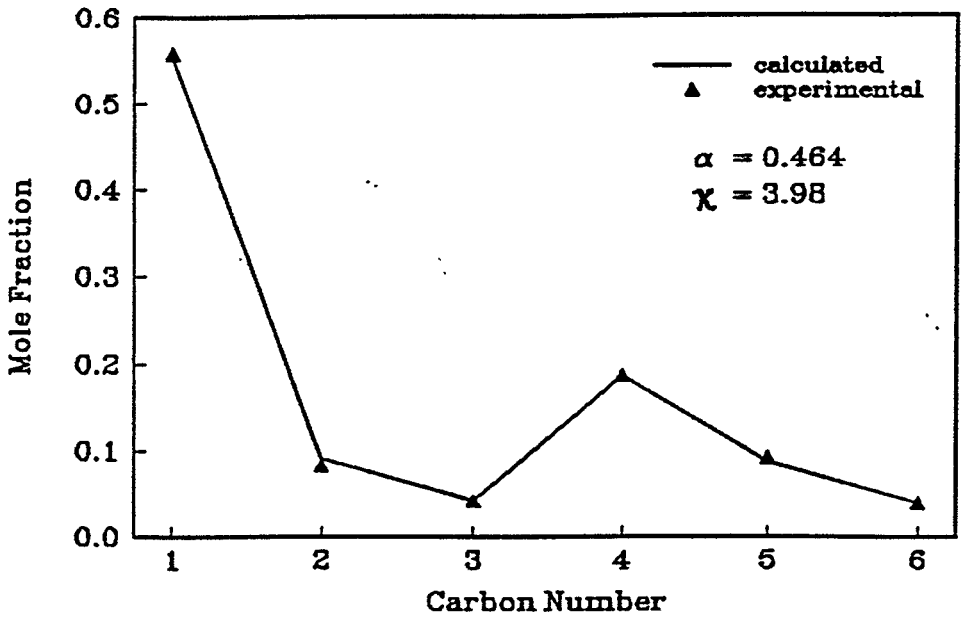

Figure 3.73. Product distribution generated by the semi-empirical model over K-ZrO_2 (MSG), at 723 K, 70 atm, 1/1 CO/H_2 ratio, and 80 second space time.

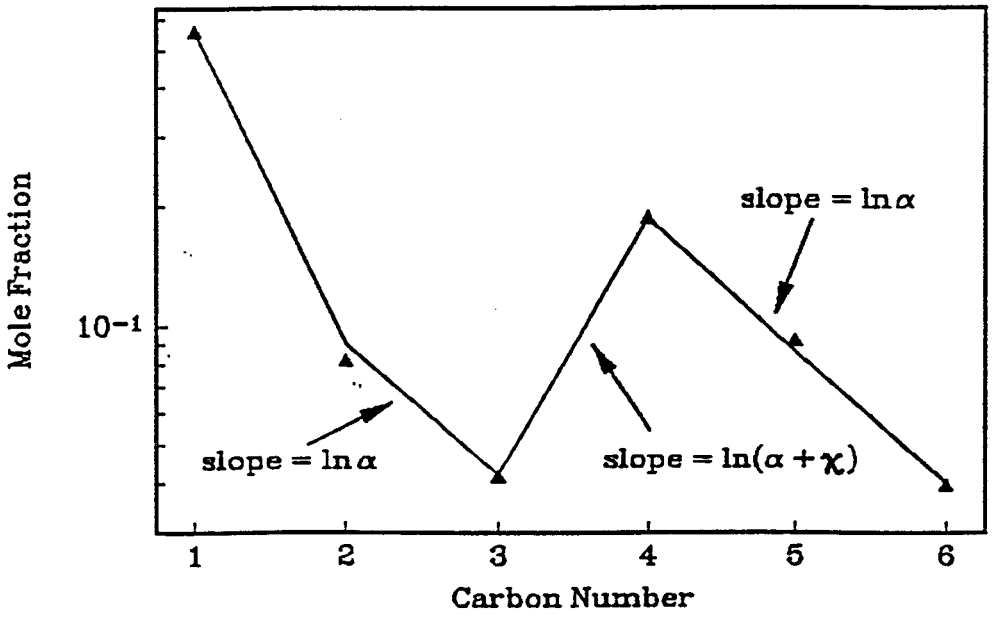

Figure 3.74. Parameters in the semi-empirical model. The distribution in Figure 3.73 is plotted on a semi-log scale, and α and κ are related to the slopes of the line segments.

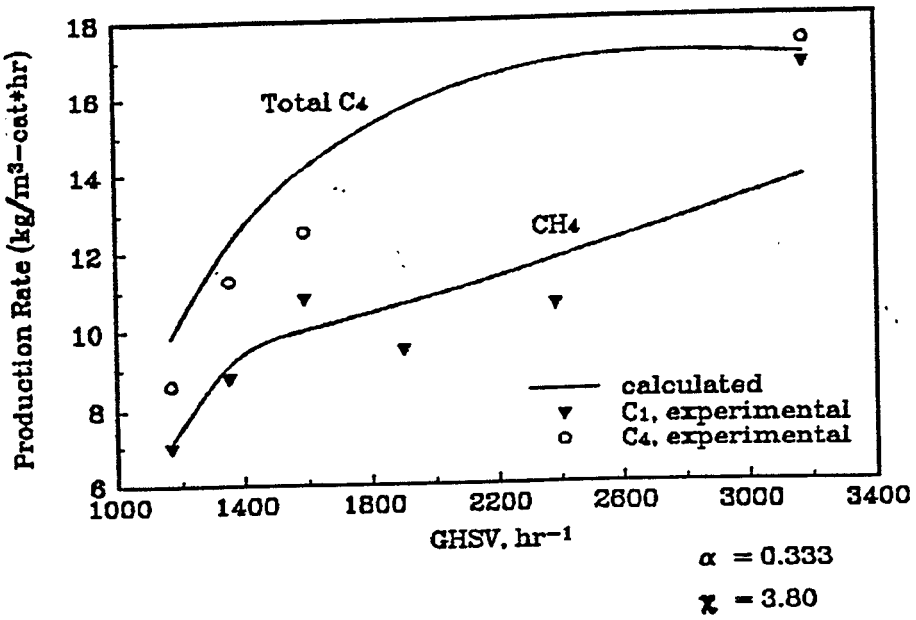

Figure 3.75. Production rates of CH_4 and C_4 hydrocarbons. Calculated by combining the semi-empirical model for hydrocarbon distribution with the empirical CO reaction rate. ZrO_2 (H-0304), 723 K, 70 atm, 1/1 CO/H_2 ratio.

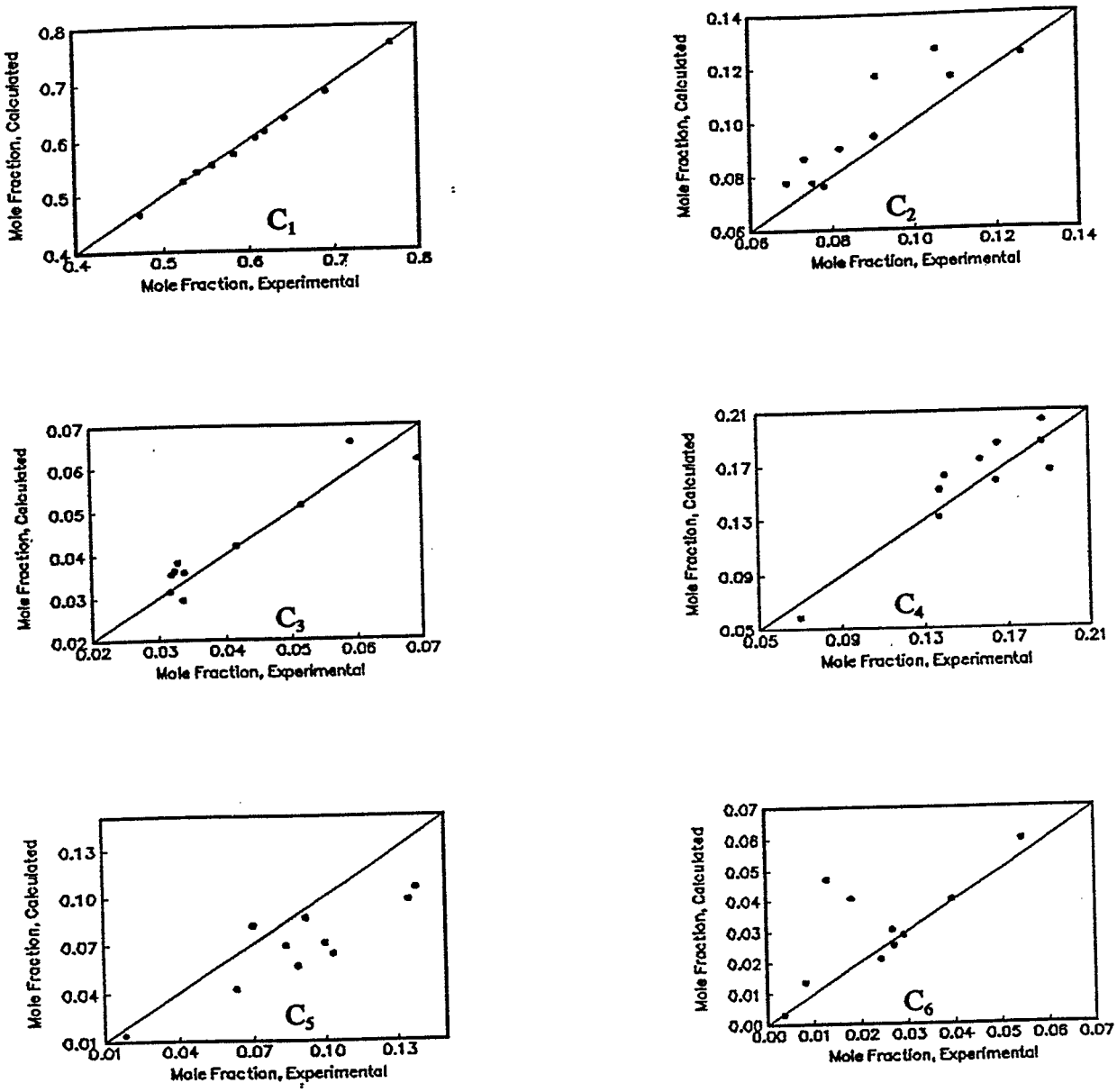

Figure 3.76. Residual plots for hydrocarbon distributions. For all the catalysts in Table 3.30 at 723 K, 70 atm, and 20 to 80 second space times.